



HAL
open science

The epidemiological footprint of contact structures in models with two levels of mixing

Vincent Bansaye, François Deslandes, Madeleine Kubasch, Elisabeta Vergu

► **To cite this version:**

Vincent Bansaye, François Deslandes, Madeleine Kubasch, Elisabeta Vergu. The epidemiological footprint of contact structures in models with two levels of mixing. 2023. hal-04012906v1

HAL Id: hal-04012906

<https://hal.science/hal-04012906v1>

Preprint submitted on 7 Mar 2023 (v1), last revised 21 Feb 2024 (v2)

HAL is a multi-disciplinary open access archive for the deposit and dissemination of scientific research documents, whether they are published or not. The documents may come from teaching and research institutions in France or abroad, or from public or private research centers.

L'archive ouverte pluridisciplinaire **HAL**, est destinée au dépôt et à la diffusion de documents scientifiques de niveau recherche, publiés ou non, émanant des établissements d'enseignement et de recherche français ou étrangers, des laboratoires publics ou privés.

The epidemiological footprint of contact structures in models with two levels of mixing

Vincent Bansaye¹, François Deslandes², Madeleine Kubasch^{1,2}, Elisabeta Vergu²

¹Ecole Polytechnique, Centre de mathématiques appliquées (CMAP), 91128 Palaiseau, France

²MaIAGE, INRAE, Université Paris-Saclay, 78350 Jouy-en-Josas, France

Abstract

Models with several levels of mixing (households, workplaces), as well as various corresponding formulations for R_0 , have been proposed in the literature. However, little attention has been paid to the impact of the distribution of the population size within social structures, effect that can help plan effective interventions. We focus on the influence on the model outcomes of teleworking strategies, consisting in reshaping the distribution of workplace sizes. We consider a stochastic *SIR* model with two levels of mixing, accounting for a uniformly mixing general population, each individual belonging also to a household and a workplace. The variance of the workplace size distribution appears to be a good proxy for the impact of this distribution on key outcomes of the epidemic, such as epidemic size and peak. In particular, our findings suggest that strategies where the proportion of individuals teleworking depends sublinearly on the size of the workplace outperform the strategy with linear dependence. Besides, one drawback of the model with multiple levels of mixing is its complexity, raising interest in a reduced model. We propose an unstructured *SIR* ODE-based model, explicitly exhibiting social structure sizes. This reduced model, sharing the same growth rate as the initial model, yields a generally satisfying approximation of the epidemic. These results, robust to various changes in model structure, are very promising from the perspective of implementing effective strategies based on social distancing of specific contacts. Furthermore, they contribute to the effort of building relevant approximations of individual based models at intermediate scales.

Key words: Epidemic process, household-workplace models, two layers of mixing, overlapping groups, epidemic growth rate, teleworking strategies, model reduction.

1 Introduction

The dynamics of an epidemic relies on the contacts between susceptible and infected individuals in the population. The number and characteristics of contacts has a major quantitative effect on the epidemic. In addition to the main features playing a role in the description of contacts, such as the age and propensity to travel of individuals [12, 18], the nature of the contact is also crucial: homogeneous mixing in closed structures (household, workplaces, schools,...) or related to other intermediate social structures (group of friends, neighbors...) e.g. [20]. The heterogeneity of contacts can be captured in network based models [21] or models with multiple levels of mixing, more precisely models with two levels of mixing, *i.e.* considering global mixing within the population at large and uniform mixing within each element of a population partition, the population being partitioned in several ways, called also overlapping groups [4]. These modeling frameworks or their simplified unstructured versions allow to tackle important questions related to the control of epidemic dynamics by acting specifically on these different population structures. Furthermore, the computation of the corresponding reproduction number R_0 , arguably one of the most important epidemic indicators, enables to assess control measures.

For the homogeneous mixing *SIR* model, several important characteristics can be summarized by R_0 . This threshold parameter indicates whether there will be a large epidemic outbreak, allows to calculate the final epidemic size and the fraction of the population that needs to be vaccinated in order to stop an outbreak, see e.g. Ball *et al.* [5]. It is also directly linked to the exponential growth rate r at the beginning of the epidemic, and has a clear interpretation as the mean number of individuals contaminated by a single infected individual in a large susceptible population. For models with two levels of mixing (*e.g.* household-workplace models), however, the definition of a unique reproduction number combining these criteria has not been achieved yet. Instead, various reproduction numbers have been proposed, of which Ball *et al.* [5] have given an interesting overview. All of them respect the threshold of 1 for large epidemic outbreaks, and they generalize one or another aspect of the traditional R_0 . Some of these reproduction numbers have the advantage of an intuitive interpretation. This is the case of the reproduction number R_I introduced by Pellis *et al.* in the supplementary material of [25]. It is defined using a three-type process, where individuals can either be infected through the general population, in their household or at their workplace. Within a closed structure, the primary infected is considered responsible for all subsequent cases. Thus, an individual who has been infected in his household is regarded as causing all infections within his workplace but none within his household. The counterpart occurs for infections in workplaces. An individual infected through the general population is responsible for all infections within his household and workplace. Some correlation between the numbers of infections an individual causes in his household and workplace (see [7]), which is due to the infectious period being identical in both structures he/she belongs to, will be neglected. This procedure groups infected individuals into generations where each infected individual is replaced independently from one generation to the following by a random number of individuals of each type, who are considered his offspring. The distribution of his offspring depends solely on the type of the infected. The process is then a discrete time multi-type branching process, and its expectation satisfies a linear induction. Then R_I is defined as the Perron root of the corresponding square matrix of dimension 3.

Nevertheless, a drawback of most of the reproduction numbers for household-workplace models that are described by Ball *et al.* [5] is that by construction, they lose track of time. Indeed, in an effort to construct meaningful generations of infected individuals, the timing of the infections is neglected. As a consequence, contrary to the case of homogeneous mixing, there is no simple link between these reproduction numbers and the initial exponential growth rate. The only exception is R_r , a reproduction number which has originally been introduced by Goldstein *et al.* [19] for household models, and whose definition has been extended by Ball *et al.* to household-workplace models [5]. The definition of this reproduction number depends explicitly on r . But as far as we see, it has no easy intuitive interpretation. It thus seems pertinent to complement the information yielded by a reproduction number such as R_I with the exponential growth rate r . While simple closed analytic expressions seem out of reach, Pellis *et al.* [26] have obtained an interesting characterization that we use and complement by more explicit expressions. Given the relative difficulty for computing reproduction numbers for models with several levels of mixing, Goldstein *et al.* [19] have suggested, in the case of the simplest model with two levels of mixing, namely structured only in general population and households, to first estimate the growth rate from data, and to then compute R_r , since the only other information required concerns the infectious process at the general population level. Trapman *et al.* [29] have gone one step further, by proposing to first infer r from data, and then totally neglect the population structure and approximate a reproduction number from r using the formula linking the reproduction number to the exponential growth rate in the homogeneous mixing model. They find that this procedure is generally satisfactory.

All this makes one wonder to what extent it is possible in general to approach an epidemic spreading in a household-workplace model by a simple, unstructured, well parametrized com-

partmental model. Some work has been done in this direction by del Valle Rafo *et al.* [13]. They have shown that it is possible to approach an *SIRS* household-workplace model by a homogeneously mixing *SIYRS* model, where *Y* stands for infected but no longer infectious individuals, once the parameters have been well chosen. Similarly, they find that the Ross-MacDonald model assuming homogeneous mixing captures the essential dynamics of vector-borne diseases on household-workplace models. In our case, we are interested in an *effective SIR homogeneous mixing model*, which would keep track of the social organization through the infectivity parameter, without adding additional variables or parameters to the classical three dimensional *SIR* differential equations. Naturally, a related question is to understand the way this social organisation characterized by small contact structures has an impact on the major features of an epidemic.

From the point of view of control, an advantage of the household-workplace model is that it is a minimal model allowing to account for closures of schools and workplaces. For the past years, governments world-wide have implemented such non-pharmaceutical interventions (NPIs) in reaction to the COVID-19 epidemic. Since then, several studies have assessed the impact of these measures on the epidemic spread. Mendez-Brito *et al.* [23] have analyzed the findings of 34 empirical studies, and pointed out that (partial) school closures and home working are among the most effective measures regarding incidence reduction. These conclusions are in accordance with those of simulation studies. For instance, Backhausz *et al.* [2] have explored through simulations a model taking into account age structure, spatial structure and several levels of mixing: households, schools subdivided in smaller groups representing classes, workplaces and community contacts. They have found that especially closure of schools has a major impact on the epidemic, while home working did not have a significant effect, which should be balanced by the fact that only workplaces of small sizes were considered. Similarly, Simoy and Aparicio [28] have proposed an agent-based model for COVID-19 and implemented several combinations of NPIs. They have found that in some epidemic scenarios, both school closure and the closure of a fraction of workplaces are necessary to maintain the epidemic below a critical level for health systems of reduced capacity. Together, these findings motivate an interest in mathematical models enabling a closer study of school and workplace closures, and more generally the effect of control measures targeting small contact structures.

In this paper, based on a stochastic *SIR* model including two types of structures and two levels of mixing, we are interested in the impact of the distribution of individuals in closed structures on epidemic dynamics. In particular, we are motivated by and study the impact of several control policies based on differentiated social distancing. For some structures, in particular for households, it is natural to assume that their size distribution is fixed and control policies cannot act on it. For others, such as workplaces and schools, control measures aiming at contact reduction can be considered, COVID-19 epidemic having raised this issue in new manners. Focusing on workplaces, we study here how control strategies such as teleworking strategies, which consist in modifying the structures' size distribution, can impact the epidemic dynamics. We measure this impact on different epidemic outcomes, among which a reproduction number R_0 , for which we make use of the definition proposed by Pellis *et al.* [25] that was previously introduced as R_I . We will see that this reproduction number has the advantage of being connected to further relevant information on the household-workplace epidemic, namely the proportions of infections occurring at each level of mixing. More generally, we demonstrate through simulations that the size distribution of closed structures has a significant effect on epidemic dynamics, as assessed by the total number of infections, the initial growth rate of infection, and maximal number of infected individuals along time. In particular, when both the number of individuals and structures is fixed, implying that the average structure size is constant as well, we show that these epidemic outcomes are sensitive to the variance of the structure size distribution. In short, balancing structure sizes reduces the impact of the epidemic.

One drawback of the model with two levels of mixing is that numerical simulations rely on good knowledge of several epidemic parameters, such as the rates of infection within each level, which may not be easy to assess. However, considering the significant impact of structure size distributions on epidemic outcomes and the fact that control measures may actively impact these distributions, it seems crucial not to neglect this particular population structure. This motivates the development of reduced epidemic models, which aim to be more parsimonious, while still being able to capture the impact of small structures on the epidemic thanks to a pertinent choice of parameters. Here, we propose such a reduced model, that we evaluate using simulations. We will see that the initial growth rate is the key parameter for reducing the full epidemic process at the macroscopic level.

The questions we consider here involve quantities which capture some main features of the epidemics. These key epidemic indicators are relevant for specific phases of an epidemic, which are recalled hereafter. Starting from a single infectious individual in a large population of size N , epidemic dynamics can be decomposed into three phases. This holds and has been proved for simple model such as the homogeneously mixing *SIR* model. In the following, we will detail these phases for this model, letting β denote the contact rate and γ the removal rate. However, notice that this decomposition still holds in more complex models, including the model with two levels of mixing studied here.

Phase 1: random behavior in small population. When the number of infected individuals $I(t)$ is of order 1, i.e. $I(t) = O(1)$, $I(t)$ is approximated by a linear birth and death process. This approximation holds on finite time intervals but also up to a time T_N which tends to infinity when N tends to infinity. More precisely, both processes coincide as long as the number of infected individuals is below \sqrt{N} [6]. Let us also mention [9], for comparison results, until the infected population reaches sizes of order of $N^{2/3}$, for a discrete time counterpart of the *SIR* model.

Phase 2: deterministic evolution and linear behavior. When $1 \ll I(s), I(t) \ll N$, the number of infected follows a deterministic and exponential dynamic: $I(t) = I(s)e^{(\beta-\gamma)(t-s)}$, where β is the transmission rate and γ the recovery rate. This approximation is valid as soon as s, t tend to infinity but remain far from the time $\log(N)/(\beta - \gamma)$, which corresponds to the entry in the macroscopic level. This deterministic phase allows to capture the initial growth rate of infection, $\beta - \gamma$, by considering the slope of the growth of I on a logarithmic scale.

Phase 3: macroscopic deterministic behavior. When the number of infected individuals is of order N , i.e. $I(t) = O(N)$, after renormalization by N , the number of susceptible, infected and recovered individuals can be approximated by a macroscopic deterministic system. More precisely, letting N go to infinity, the trajectories of $(S/N, I/N, R/N)$ converge in law on finite time intervals to the solutions of the *SIR* dynamic system. The approximation is valid for any t greater than $\log(N)/(\beta - \gamma)$. For accurate results, we refer in particular to [8]. Let us also mention that fluctuations around the deterministic curve are of order $1/\sqrt{N}$ by classical Gaussian approximation [15].

In our study, *phase 1* corresponds to the regime where stochasticity of the individual-based version of the *SIR* model is observed in simulations. *Phase 2* is the relevant regime for the definition of R_0 and the initial growth rate r . *Phase 3* yields the deterministic macroscopic approximation, where stochasticity vanishes. This phase is the one involved in the reduction we consider. It starts at a random time necessary to reach a macroscopic proportion of infected. This time represents the starting point of the comparison between the stochastic structured model to its reduced ODE-based counterpart we propose.

This paper is structured as follows. Section 2 presents the main modeling ingredients, such as a detailed description of the model with two levels of mixing and proper introduction of considered key parameters, as well as numerical settings for simulations. Section 3 is devoted to the study of the impact of the structure size distribution on some main epidemic outcomes,

namely the reproduction number, the exponential growth rate, the peak size and the final epidemic size. For this purpose, two slightly different situations are considered. While the size of the population is always considered fixed, we first keep the total number of workplaces constant as well but vary the way individuals are distributed among these given workplaces, see Section 3.2. Second, we consider teleworking strategies, which differ from the previous setting as for simulations, these strategies amount to creating a new workplace of size one for each teleworking employee, see Section 3.3. The robustness of these results is roughly addressed in Section 3.4. Finally, in Section 4, we propose an ODE reduction of the initial multi-level model based on the computation of the initial growth rate and assess its robustness. The paper concludes with a discussion (Section 5) of the main results on the impact of structure size distributions on epidemic dynamics, their robustness to different modeling assumptions, and their implications for control measures.

2 Model with two levels of mixing: description, simulation approach, key parameters, simulation scenarios

2.1 General model description

We consider an *SIR*-type model with two levels of mixing by considering global and two types of local contacts following two local partitions of the population, see [4]. In addition to homogeneous mixing in the general population, contacts occur in households and workplaces of various sizes, in which the population is structured. Each individual belongs both to a household and a workplace, which are chosen independently from one another. Generally speaking, infection spreads through contacts between susceptible and infected individuals within each level of mixing, which are characterized by different contact rates among individuals as will be detailed below. Infected individuals recover at rate γ .

We distinguish two slightly different types of parametrization concerning contact description. For closed structures such as households and workplaces, we will use *one-to-one* infectious contact rates λ_H and λ_W , respectively. In other words, within a household, if there are s susceptibles and i infected individuals, each susceptible is infected at rate $\lambda_H i$ (resp. $\lambda_W i$ for workplaces). This has the disadvantage to make the average number of contacts established by each individual grow with the size of the structure. This is tractable for structures of finite size, and a good enough approximation of contacts within very small structures, but it is not realistic at the scale of the general population. Instead, within the general population, when there are s susceptibles and i infectious individuals, each susceptible individual becomes infected at rate $\beta_G i / (N - 1)$ where N is the population size. Here, the parameter β_G represents the *one-to-all* infectious contact rate, which is the global rate at which an infected individual makes contact with all other individuals in the population. Hence the corresponding one-to-one infectious contact rate $\lambda_G^{(N)} = \beta_G / (N - 1)$ is small. This allows to scale the contact rates when N tends towards infinity, so that the mean number of contacts made by an infected individual remains constant. The global speed of infection in the population is then $\beta_G IS / (N - 1) = \lambda_G^{(N)} IS$ where S (resp. I) is the number of susceptible (resp. infected) individuals, and S is indeed of order N .

2.2 Structure size distributions

Let us introduce the size distribution of households and workplaces, called π^H and π^W , respectively. When the number of structures is large, π_k^H (resp. π_k^W) is the proportion of households (resp. workplaces) of size $k \geq 1$. The total number of individuals is N , which is fixed. Besides, all individuals belong to one (and only one) household and workplace, the latter being of size

one for teleworking employees. Notice that

$$N = N_H \sum_{k \geq 1} k \pi_k^H = N_W \sum_{k \geq 1} k \pi_k^W$$

where N_H (resp. N_W) is the total number of households (resp. workplaces). We define $m_H = \sum_{k \geq 1} k \pi_k^H$ (resp. $m_W = \sum_{k \geq 1} k \pi_k^W$) the average household (resp. workplace) size.

Distributions of a given mean, variance and maximum size were generated using the following algorithm: (1) create an initial set of distributions with the given mean and variance using only two sizes; the support of the size distribution is reduced to two integers below the maximal value. (2) create random mixtures of these distributions from step (1), which keep the same mean and variance by linearity (these quantities are stable by convex combination). This procedure was sufficient to cover a wide range of distribution shapes.

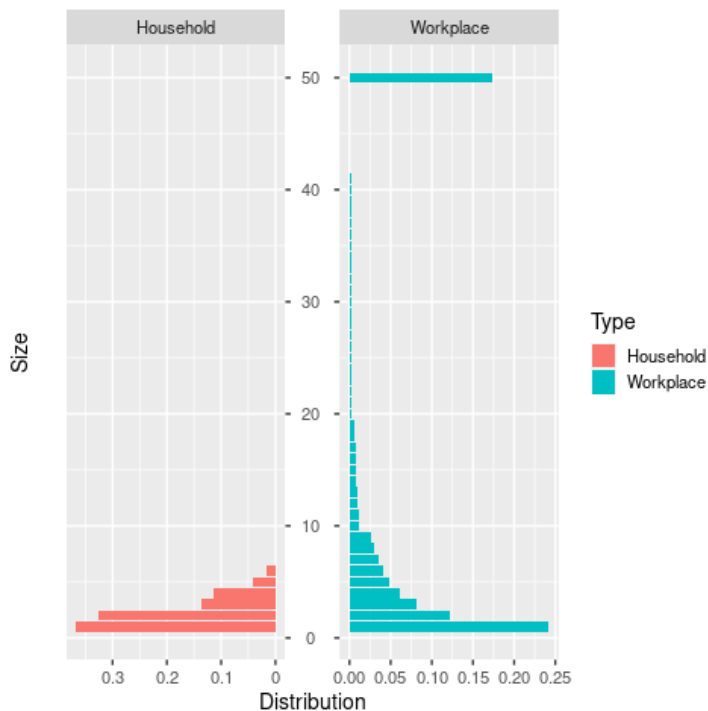


Figure 2.1: Reference households size distribution (red) corresponding to the size distribution of households in France in 2018. Reference workplace size distribution (green) derived from workplace size distributions in Ile-de-France.

2.3 Simulations of the population structure and epidemic process

The epidemic process was simulated using the Gillespie algorithm (Stochastic Simulation Algorithm). A population structure (contacts between individuals) is first generated from the size distributions of households and workplaces, generated as described in Section 2.2. Individuals are listed from 1 to N and placed in structures randomly by applying the following iterative process: (i) for each type of structure, randomly select a structure size with probability given by the size distribution; (ii) randomly select the corresponding number of individuals among the individuals that have not yet been assigned to a structure of the same type. For a given population structure, the algorithm computes the rates of events, *i.e.* infection events in households, workplaces and the general population, and recovery, as described in Section 2.1. These

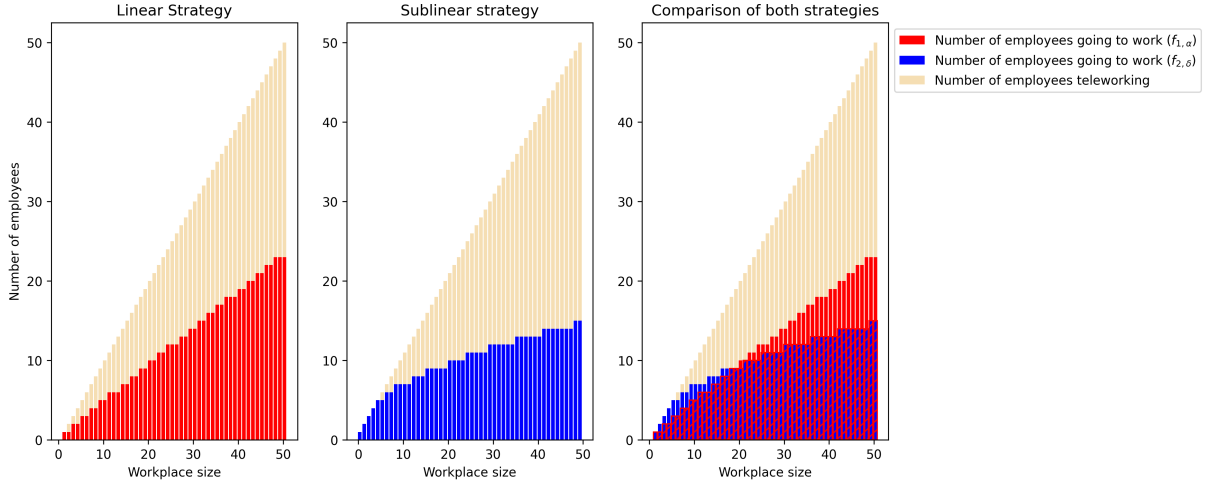


Figure 2.2: For each workplace size, number of employees coming to work on site or teleworking according to either the linear or the sublinear strategy. The parameters α and δ are chosen in order to observe an average proportion of employees teleworking per workplace equal to 0.5 for the uniform workplace size distribution ($\alpha = 0.46, \delta = 2.01$).

rates are used to derive the next event, *i.e.* infection of a susceptible individual or recovery of an infected individual, and the corresponding event time. The epidemic is initiated with a single infected individual, selected uniformly at random in the population. For each run of the epidemic process, we compute several classical summary statistics: (i) the final epidemic size, *i.e.* the number of individuals that are in the recovered state when the number of infected individuals becomes 0; (ii) the infectious peak size, *i.e.* the maximum number of infectious individuals occurring simultaneously over the course of the epidemic; (iii) the infectious peak time, *i.e.* the time at which the infectious peak occurs.

2.4 Reproduction number

The reproduction number is computed numerically using average sizes of epidemics in isolated structures obtained by simulation. For a given set of structure size, transmission parameter and recovery rate, we simulate the within structure epidemic using Gillespie's algorithm, and record the final epidemic size. We thus calculate the average size of epidemics in isolated structures from simulations of this epidemic process (default value of the number of runs: 10000, and 50000 for larger workplaces). The value of R_0 is then obtained from forthcoming Equation (3.4), as the largest eigenvalue of the matrix defined in forthcoming (3.2), by replacing unknown quantities by simulated quantities. The proportions of infections occurring within each layer of mixing are obtained from the associated eigenvector, see forthcoming Section 3.1 .

2.5 Initial growth rate

The initial growth rate can be captured in *phase 2* of the epidemic as defined in the introduction. Indeed, we can check by simulations that the course of the epidemic becomes non random, as the number of infected grows large, and non dependent on the initial choice of the infected individual. This rate will be characterized as the spectral radius of the matrix defined in forthcoming Equation (4.22), based on previous work by Pellis *et al.* [25].

2.6 Simulation of teleworking strategies

We evaluated the evolution of different epidemic outcomes for varying proportions of teleworkers using two strategies (fig. 2.2): (i) Linear strategy. The workplace size distribution is modified according to the function $f_{1,\alpha}(k) = \lceil \alpha k \rceil$, where $\lceil x \rceil = x$ when $\alpha \in [0, 1]$ and $n - 1 < x \leq n$ and $n \in \mathbb{N}$. This means that a work place of size k becomes a workplace of size $\lceil \alpha k \rceil$ and the remaining $k - \lceil \alpha k \rceil$ individuals now telework. (ii) Sublinear strategy. The workplace size distribution is modified according to the function $f_{2,\delta}(k) = \lceil \delta k^{\frac{1}{2}} \rceil \wedge k$, where $\delta \geq 0$. This means that a work place of size k becomes a workplace of size $\lceil \delta k^{\frac{1}{2}} \rceil$ and the remaining $k - \lceil \delta k^{\frac{1}{2}} \rceil$ individuals now telework.

The rationale behind the sublinear strategy is that withdrawing an individual from a large structure has a stronger impact in terms of number of contacts. Notice that we consider here the exponent $1/2$ for the sublinear strategy, but one could more generally consider any exponent $q < 1$.

2.7 Numerical simulation scenarios: structure size distributions and epidemiological parameters

In the numerical explorations of the impact of the structure size distribution on the epidemic dynamics, we use the household size distribution observed in France in 2018 as reference distribution and also more generally, unless stated otherwise. We also provide a workplace distribution corresponding to the workplace size distribution of Ile-de-France in 2018, later called reference workplace size distribution. To study the impact of the average workplace size and workplace variance we provide the following sets of exploratory workplace size distributions: (A) a set of 160 workplace distributions with mean ranging from 3 to 30, different variances and maximal size 50; (B) a set of 100 workplace distributions with mean 20, different variances and maximal size 50; (C) a set of 100 workplace distributions with mean 7, different variances and maximal size 50. These workplace size distributions were generated using random mixtures of distributions.

The sets of structure size distributions are summarized in Table 1.

Name	Number of distributions	Average size (value/range)	Variance (value/range)	Maximum size	
Reference household size distribution	1	2.2	1.6	6	
Reference workplace size distribution	1	13.8	331.5	50	
Exploratory workplace size distributions	A	160	3-30	9.8-554.3	50
	B	100	20	42.4-544.0	50
	C	100	7	5.8-248.8	50

Table 1: Household and workplace size distribution sets.

Numerical exploration of the model was performed using a combination of various epidemic parameters. We consider epidemic scenarios which differ both in terms of growth rates and in terms of proportions of infections occurring within each level of mixing. The full set of scenarios and their epidemic parameters is given in Table 2. For example, in scenario 1, the distribution of infections through households and workplaces is derived from proportions of infections reported in [16] and [17]. Scenario 2 has increased growth rate compared to scenario 1, whereas scenario 4 has a similar growth rate but higher proportion of infection through global mixing than scenario 1. Without loss of generality, the recovery rate is set to 1 in all simulations. In this case, setting desired values for R_0 , p_G , p_H and p_W is enough to set unique values for the infectious contact rates within each level of mixing. Illustration of the simulated final size for each scenario and exploratory workplace size distribution in the simulation study are provided in figure 6.1.

scenario	growth rate	R_0	p_H	p_W	p_G
1	2.4822	2.5028	0.4217	0.1788	0.3995
2	4.9937	4.6876	0.2796	0.3471	0.3732
3	0.0009	0.9923	0.4070	0.3927	0.2002
4	2.5203	3.6460	0.1521	0.1472	0.7008
5	2.5017	5.2021	0.1301	0.5445	0.3254
6	0.5054	1.5740	0.3868	0.3456	0.2676
7	0.5061	1.5187	0.1120	0.1122	0.7758
8	0.5020	1.5920	0.3975	0.4057	0.1968
9	0.1104	1.1330	0.3879	0.4182	0.1940
10	0.0900	1.0989	0.2631	0.2646	0.4723
11	0.0706	1.1068	0.3449	0.5883	0.0668

Table 2: Epidemic parameters for various simulation scenarios.

3 The impact of the size distribution of closed structures and assessment of teleworking strategies

3.1 Outbreak criterion, R_0 and type of infection

Various notions of R_0 have been proposed, as a compromise between complexity of the computations and epidemiological interpretation. The idea is to capture the mean number of infections caused more or less directly by one single "typical" individual. This concept is primarily defined in the first steps of the epidemic, which usually can be approximated by a branching process, whose mean satisfies a linear ODE. A typical individual corresponds then to a uniform sample in the corresponding population.

R_0 is delicate to define for epidemiological processes with multi-level contacts, such as the one we consider here. We recall that each infected individual infects an individual outside his structure with rate $\beta_G S / (N - 1)$, which is in the *phase 1* approximated by β_G , since the number of susceptibles S is equivalent to N . As a consequence, the mean number of individuals directly infected in the general population by a single infected individual is β_G / γ .

We follow Pellis *et al.* [25] and structure the infected population following the origin of the infection and consider successive generations of infected individuals:

$$(I_n^G, I_n^H, I_n^W)_{n \geq 0}, \quad I_n = I_n^G + I_n^H + I_n^W.$$

Processes I_n^G , resp. I_n^H and I_n^W , count the number of individuals in generation n , which have been infected through the mean field, respectively in the household and in the workplace. I_n is the total number of infected individuals in generation n . At time 0, we assume $I_0 = I_0^G = 1$. The next generation $n + 1$ of infected individuals is created by considering the number of direct infections I_{n+1}^G in the general population, plus the local epidemic triggered within structures. This process is illustrated in figure 3.1.

To compute the mean number of infections per generation, it is necessary to compute the mean number of individuals infected during the epidemic triggered by a single infected individual in a given structure. Thus, we introduce $i_H(k)$ (resp. $i_W(k)$), the average total number of infections starting from one infected individual in a closed population of size k , one-to-one contact rate λ_H (resp. λ_W) and recovery rate γ in terms of the previously introduced *SIR* framework. It corresponds to the number of infections caused by a single infected individual which introduces the epidemic into his household (resp. his workplace) of size k . Recalling that $m_H = \sum_{k \geq 1} k \pi_k^H$ (resp. $m_W = \sum_{k \geq 1} k \pi_k^W$), we define $\hat{\pi}_k^H = k \pi_k^H / m_H$ (resp. $\hat{\pi}_k^W = k \pi_k^W / m_W$) as the size biased distribution of structure sizes, which naturally defines the household (resp.

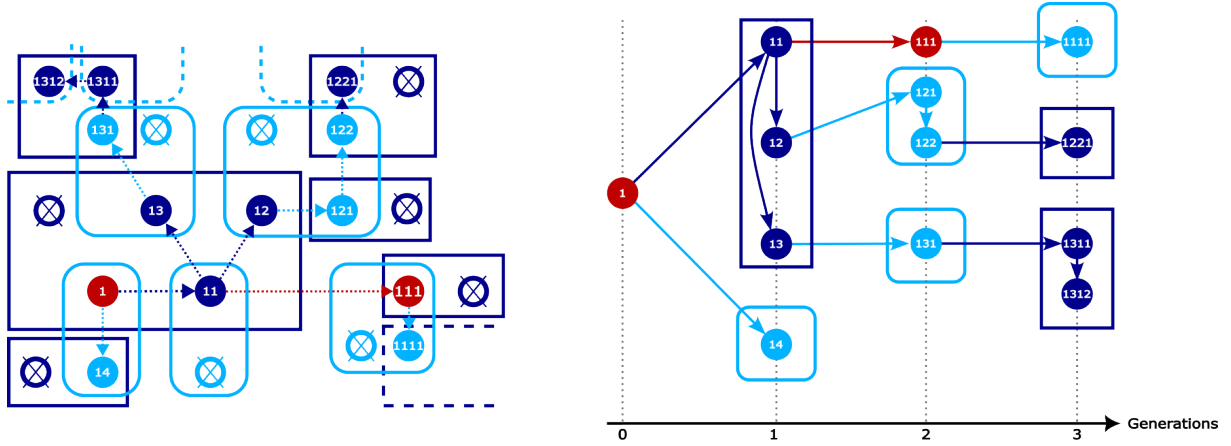


Figure 3.1: Example of an epidemic with two levels of mixing (in general population and within structures). The spread of the epidemic is shown on the left. Households and workplaces are delimited respectively in dark and light blue. Only structures containing infected individuals are shown. Individuals who have been infected during the epidemic appear as plain dots, whose colors indicate the means by which the infection occurred: through the general population (red), within households (dark blue) or within workplaces (light blue). The arrows keep track of the spread of the disease, pointing from the infector to the newly infected. Their color refers again to the type of infection. Members of a structure who have not been infected during the within-structure epidemic are represented as crossed circles. In the case of the branching model, they are never going to be infected, as a secondary introduction of the disease in an already infected structure is negligible at the beginning of the epidemic. The different generations of infected as seen by the branching process are represented on the right. Colors still encode the way each infected is contaminated, and arrows represent the true order of infections as depicted on the left. The branching genealogy is depicted through lexicographic labeling of individuals. Labels have been reported on the left panel, as to simplify identification of infected individuals in both means of representation.

workplace) size distribution of an individual chosen uniformly at random in the population. Then the numbers of infected individuals at each level triggered by an infected individual whose size structure is distributed according to the size biased law are defined by:

$$\mathcal{I}_G = \frac{\beta_G}{\gamma}, \quad \mathcal{I}_H = \sum_k \hat{\pi}_k^H i_H(k), \quad \mathcal{I}_W = \sum_k \hat{\pi}_k^W i_W(k). \quad (3.1)$$

Following Pellis *et al.* [25], the expectation $\mathbb{E}((I_n^G, I_n^H, I_n^W)^T)$ can be approximated by a sequence X_n satisfying the following linear induction

$$X_{n+1} = AX_n$$

where A is the mean reproduction matrix:

$$A = \begin{pmatrix} \mathcal{I}_G & \mathcal{I}_G & \mathcal{I}_G \\ \mathcal{I}_H & 0 & \mathcal{I}_H \\ \mathcal{I}_W & \mathcal{I}_W & 0 \end{pmatrix}. \quad (3.2)$$

As A is a primitive matrix, Perron Frobenius theorem yields the asymptotic behavior of $X_n = A^n X_0$ using its positive eigenlements, see [1]. More precisely, the unique positive vector $P = (p_G, p_H, p_W)^T$ solution of

$$AP = R_0 P, \quad p_G + p_H + p_W = 1, \quad (3.3)$$

gives the proportion of infected individuals from each source: general population, households, workplaces. The associated positive eigenvalue is

$$R_0 = \| AP \|_1$$

which corresponds to the mean reproduction number

$$R_0 = \mathcal{I}_G + (1 - p_H)\mathcal{I}_H + (1 - p_W)\mathcal{I}_W. \quad (3.4)$$

When $R_0 > 1$, the process survives with a positive probability and on this event a.s. grows geometrically fast with speed R_0 yielding a supercritical regime, under an additional moment assumption on the number of infections, see also [1]. We observe that the vector P gives the origin of the infection for large times.

R_0 can play the role of an explosion criterion, as illustrated in Figure 3.2. The final size of the epidemic is plotted against the value of R_0 for three parameter sets (scenarios 9, 10 and 11 in Table 2). These epidemic parameter sets, combined with the set of workplace size distributions, allow to cover a large range of values for p_G , p_H and p_W (more precisely, p_G between 0 and 0.5 and p_W between 0.05 and 0.65). Figure 3.2 shows that R_0 is a relevant explosion criterion.

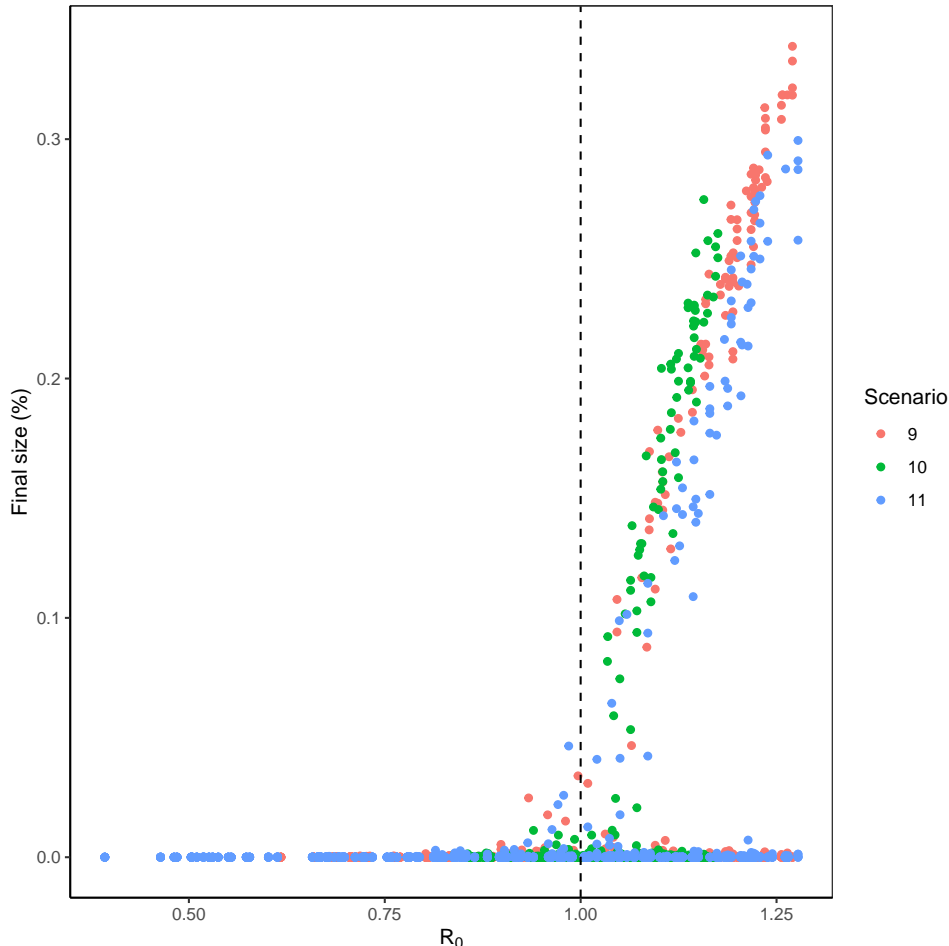


Figure 3.2: Simulated values of the final size of epidemics of the stochastic structured model as a function of R_0 . Simulations are performed for the reference household distribution, exploratory workplace size distributions from set A in Table 1 and epidemiological scenarios 9, 10 and 11 from table 2. For each combination of workplace size distribution and epidemic scenario, 10 runs are performed.

3.2 The effect of structure size distribution on epidemic outcomes

In this section, we will consider both the number of individuals and the number of workplaces as fixed. For the latter, one can imagine that this is due to logistic constraints, as there are only a certain number of offices (or classrooms) to dispose of. In other words, we are interested in understanding the epidemic impact of the way employees are assigned to those given workplaces.

From the previous section, one may notice that the workplace size distribution has a direct impact on R_0 through \mathcal{I}_W , *i.e.* the average number of infections occurring within workplaces, when the size of the workplaces is distributed according to the size-biased distribution $\hat{\pi}^W$. In particular, diminishing \mathcal{I}_W is enough to ensure that R_0 is non increasing. The average number of infected $i_W(k)$ caused by a within-workplace epidemic in a workplace of size k can be reasonably approached in some scenarios by a linear function of the workplace size k , from which we deduce that, up to a constant c ,

$$\mathcal{I}_W = \sum_{k \geq 1} \hat{\pi}_k^W i_W(k) \approx c \sum_{k \geq 1} \hat{\pi}_k^W k = \frac{c}{m_W} \sum_{k \geq 1} k^2 \pi_k^W = c \frac{m_W^{(2)}}{m_W}, \quad (3.5)$$

where $m_W^{(2)}$ designates the second moment of the workplace size distribution.

Since we suppose both the population size and the number of workplaces to be fixed, it follows that the average workplace size m_W is constant as well. As thus, in order to reduce \mathcal{I}_W , it is enough to reduce $m_W^{(2)}$. At fixed expected workplace size, modifying $m_W^{(2)}$ is strictly equivalent to modifying the workplace size variance. Since the latter has a more direct and intuitive interpretation, we will focus on the variance of π^W as a natural candidate for the epidemic impact of the workplace size distribution.

In order to assess this impact, we will proceed by numerical exploration. A variety of workplace size distributions of average fixed at 20 and different variances have been considered, corresponding to exploratory workplace size distributions set B of table 1. For each of these distributions and for epidemic scenarios 1, 2, 4 and 5 we have computed the epidemic growth rate as explained in Section 2.5, before evaluating through simulations the epidemic size and the peak size. Results have been reported in Figure 3.3 (and Figure 6.2 for additional scenarios), which thus illustrates the impact of the variance of the workplace size distributions on our selected epidemic outcomes (growth rate, final size, and peak size). This figure shows that the workplace size variance has a linear impact on these epidemic outcomes, observed for various values of average workplace size, see also Figures 6.3 and 6.4. Thus, the variance appears as a relevant indicator of the epidemic impact of the workplace size distribution. This also is of interest for the design of efficient control policies such as teleworking and (partial) closure of schools, as will be explored in the next section.

3.3 Teleworking strategies

Teleworking, a strategy to mitigate disease outbreaks, results in changes in the distribution of workplace size. These changes have an impact on the value of R_0 , which has been shown to be a threshold criterion for epidemics, and more generally on the different epidemic outcomes.

Two teleworking strategies, formalized in Section 2.6, were assessed: (i) a linear strategy, where the same proportion of teleworking is applied equally to all workplaces, and (ii) a sub-linear strategy where teleworking is more prevalent in larger workplaces. The motivation for such a strategy is twofold: larger workplaces are expected to be better equipped to mitigate the economic impact of teleworking on the firm. We will indeed show that such a strategy has a beneficial health outcome.

Figure 3.4 illustrates the behaviour of the two teleworking strategies as a function of the teleworking rate, which is defined as the proportion of individuals in the population that do not

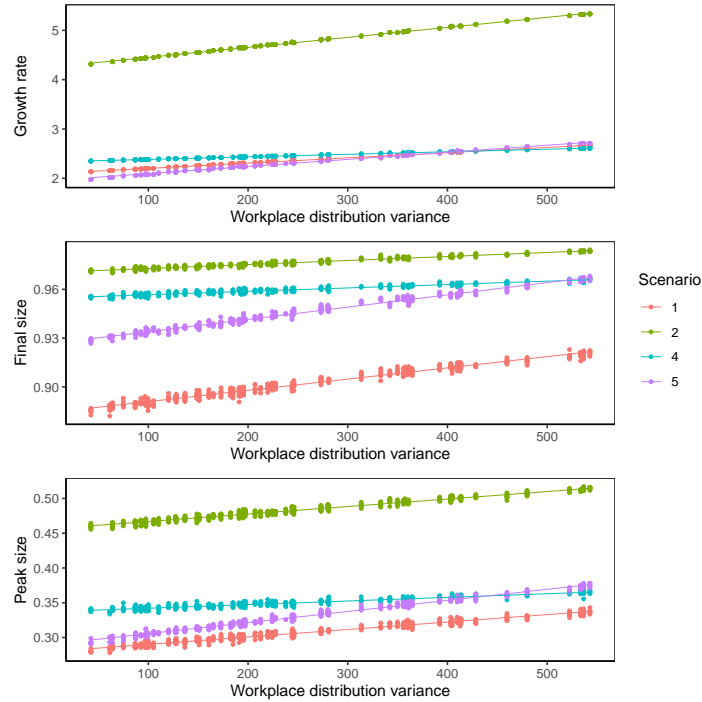


Figure 3.3: Influence of the variance of the workplace size distribution on the growth rate (top), epidemic final size (middle) and epidemic peak size (bottom). Simulations of the stochastic structured model were performed with the reference household size distribution, exploratory workplace size distribution set B with average workplace size of 20 from table 1 and epidemic scenario 1, 2, 4 and 5 from table 2. Simulations were repeated 10 times for each combination of scenario and workplace size distribution.

have contacts in a workplace. Implementation of the teleworking strategies consists in adjusting parameters α and δ from Section 2.6 to obtain a prescribed value of the teleworking rate. The proportions of infections in the different structures are the same for both strategies at the threshold $R_0 = 1$. The findings show a large reduction in the proportion of infections occurring in the workplaces. The sub-linear strategy reaches the threshold for a lower teleworking rate, which indicates that this strategy has a lower impact on workplace organisation for similar epidemic outcomes.

Figure 3.5 illustrates, for the reference workplace size distribution and epidemic scenario 1 of table 2, that even if the threshold cannot be reached by simply applying teleworking strategies, the sub-linear strategy still outperforms the linear one. In particular, it shows that for the same global teleworking rate, the final size of the epidemic is lower for the sub-linear strategy. In other words, using sublinear teleworking policies (and more generally sublinear strategies for the closure of structures) allows either to reduce the need of teleworking in order to attain a given epidemiological outcome, or to reduce more strongly the epidemiological outcome for a given teleworking rate. Both effects may even be combined: more people go to work, but the epidemic outcome is reduced when compared to the linear strategy.

3.4 Robustness to the form of the interaction term

The observed linear effect of variance on the peak size and final size of the epidemic remains valid when the model is modified to use a sub-linear infection rate in households and workplaces. In this simulation study, we focus on having an infection rate within social structures proportional to the square root of the number of infected individuals in the structures. Figure 3.6 shows the effect of the variance of the workplace size distribution with fixed mean on the epidemic

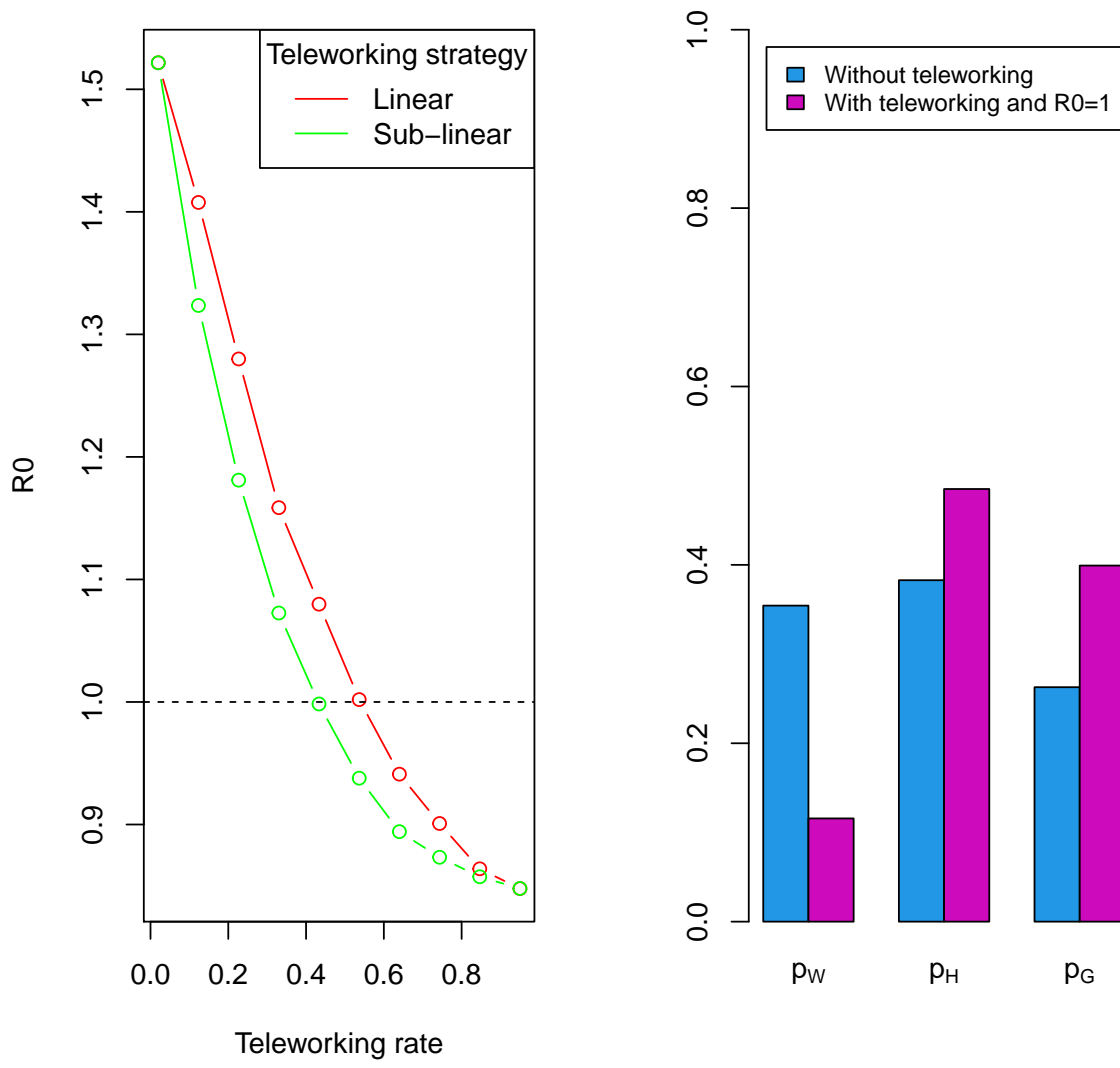


Figure 3.4: Effect of linear and sublinear teleworking strategies, using scenario 6 from Table 2 and reference household and workplace distributions from Table 1. Diminution of R_0 as a function of teleworking rate (left) and proportions of infection in the different structures (right).

outcomes for several scenarios (additional results for other scenarios can be found in Figure 6.5). This impact of the variance appears to hold for all scenarios, suggesting that the effect holds true regardless of both the epidemic speed and the proportions of infections that occur within structures. We also confirmed the validity of this result for workplace distributions with smaller mean sizes, as illustrated in Figures 6.6 and 6.7.

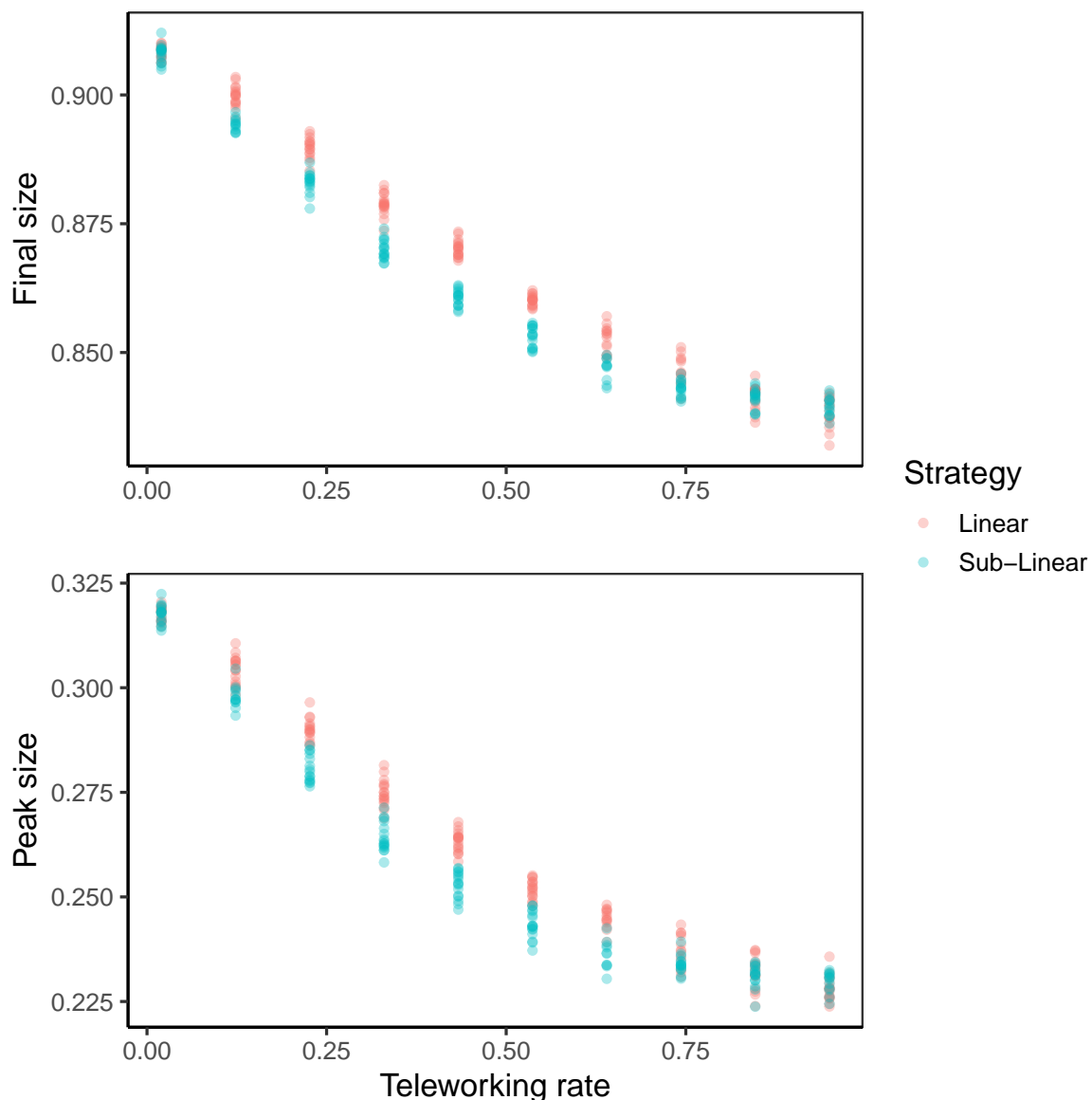


Figure 3.5: Impact of linear and sublinear teleworking strategies on the final epidemic size (top) and epidemic peak size (bottom). Simulations of the stochastic structured model were performed using the reference household size distribution and workplace size distribution from table 1, with epidemic parameters from scenarios in 1 of Table 2. 10 runs of were performed for each simulation scenario and distribution.

4 Reduction to compartmental ODEs based on the initial growth rate

In this section, our aim is to propose a relevant reduction of the multi-level contact process, when the total population is large ($N \gg 1$) and the number of infected individuals too, corresponding to *phase 2* and *phase 3* presented in the introduction. We propose a deterministic reduction which keeps track of the multi-level structuring of contacts, but has a low dimension and depends on few parameters only. It thus allows to see the effect of structure size distributions and control policies modifying them at a low computational cost. We show that the key parameter to achieve this reduction is the initial growth rate. As expected, it captures the initial growth of the size of

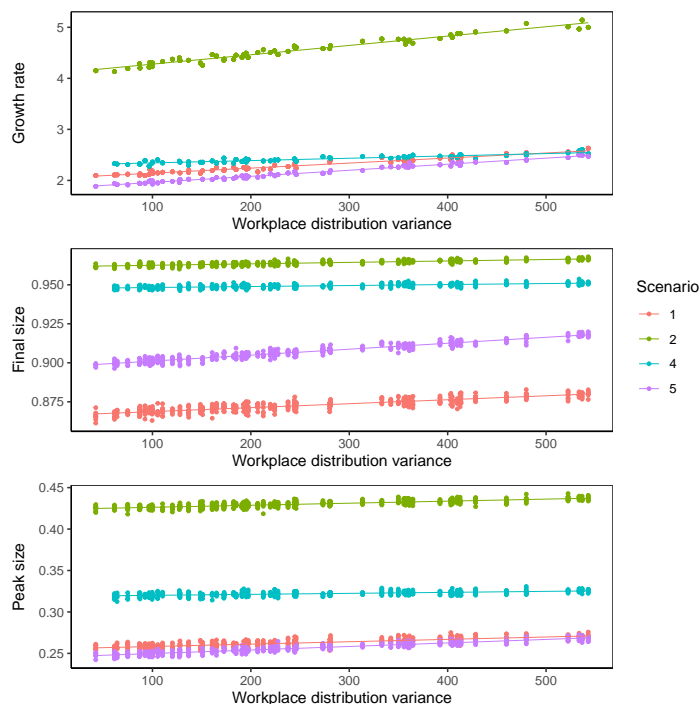


Figure 3.6: Influence of the variance of the workplace size distribution on the growth rate (top), epidemic final size (middle) and epidemic peak size (bottom). Simulations of the stochastic structured model with sub-linear infection rates in households and workplaces were performed with the reference household size distribution, exploratory workplace size distribution set B with average workplace size of 20 from table 1 and epidemic scenarios 1, 2, 4 and 5 from table 2. Simulations were repeated 10 times for each combination of scenario and workplace size distribution.

the infected population. Actually, simulations show that it also allows for a relevant prediction of the rest of the epidemic, see Section 4.3 for details on the interest and limitations of this reduction.

We assume that the total population size N is large and consider an approximation in an infinite population. As for the branching approximation considered in Section 3, we focus on the beginning of the epidemic (*phase 1* and *phase 2*). As households and workplaces are chosen independently from one another and for each individual, this implies that whenever an infection occurs in the general population, it will almost surely affect an individual whose household and workplace are entirely susceptible otherwise. Similarly, an infection taking place within a household will cause an infection within an otherwise susceptible workplace, and vice-versa. Some time is needed to reach a large (but still negligible compared to N) number of infected individuals and forget the peculiar initial condition. Perron Frobenius theorem allows to get a deterministic growth rate, which is observable in *phase 2*. It is called the initial growth rate r . It will play a crucial role in reducing and analyzing the process in the deterministic phase with a macroscopic number of infected individuals (*phase 3*).

For the stochastic *SIR* model in large homogeneously mixing populations, the initial growth rate can readily be obtained [14]. Let us briefly explain the heuristics of the reasoning. Consider $\mathbf{i}(t)$ the number of new infections in the population occurring at time t after the start of the epidemic. It is easy to see that $\mathbf{i}(t)$ satisfies a renewal equation, which may be used to deduce an implicit equation for the exponential growth rate \bar{r} . Indeed, suppose that $\mathbf{i}(t) = Ce^{\bar{r}t}$ for some constant C , and let $\zeta(\tau)$ denote the average rate at which an individual who has been infected

τ units of time ago transmits the disease. Then \bar{r} is characterized as follows:

$$\mathfrak{L}(\zeta)(\bar{r}) := \int_0^\infty \zeta(\tau)e^{-\bar{r}\tau}d\tau = 1, \quad (4.1)$$

where \mathfrak{L} designates the Laplace transform operator. In order to conclude, it remains to make ζ explicit, and at the beginning of the epidemic, one readily obtains the approximation $\zeta(\tau) \approx \beta e^{-\gamma\tau}$. Injecting this into the implicit equation $\mathfrak{L}(\zeta)(\bar{r}) = 1$ leads to the well-known growth rate $\bar{r} = \beta - \gamma$. This derivation can rigorously be obtained using branching approximations [24].

Exponential growth of infections is also observed when household-workplace structures are added to homogeneous mixing, and Pellis *et al.* [26] characterize the associated growth rate r . Similarly to what has been done for the reproduction number, they aggregate within-structure epidemics to facilitate the mathematical analysis of the model. This leads to a point of view where an infected household contaminates a new workplace each time an infection occurs during the within-household epidemic, and vice-versa. Using equation (4.1), this allows for the exact characterization of r as the unique solution of an implicit equation, which can be solved numerically. This motivates the study of the Laplace transform (4.1) of the average rate at which infections occur during the course of within-structure epidemics, which captures the dynamics of these infections.

Here, we follow and complement the approach in [26], mainly by providing more explicit expressions of the key quantities involved. The following Section 4.1 introduces our contribution, which lies in Proposition 4.1 and its corollaries. Subsequent Section 4.2 summarizes the work of Pellis *et al.* [26], and allows to position our contribution in the context of their work.

4.1 Laplace transform of the infection rate in a uniformly mixing population

The main point lies in understanding the dynamics of the stochastic *SIR* model in a population of finite size n , with any one-to-one infectious contact rate λ and removal rate γ . The results on within-household or within-workplace epidemics will follow by choosing these parameters accordingly.

More precisely, consider the continuous-time Markov chain $X_{n,\lambda,\gamma} = (S, I)$ taking values in $\bar{\Omega}(n) = \{(s, i) \in (\mathbb{N} \cup \{0\})^2 : s + i \leq n\}$, and whose transition rates are given by

Transition	Rate	
$(s, i) \rightarrow (s - 1, i + 1)$	$\lambda si;$	(4.2)
$(s, i) \rightarrow (s, i - 1)$	$\gamma i.$	

Then S_t and I_t represent respectively the number of susceptible and infected individuals at time t . Furthermore, the initial condition of interest is $x_0^n = (n - 1, 1)$, and $\mathbb{P}_{x_0^n}$ denotes the probability conditionally on $X_{n,\lambda,\gamma}(0) = x_0^n$.

Let us start by summarizing the results obtained by Pellis *et al.* [26] on this matter. From (4.2), it is obvious that when the population is in state (s, i) , a new infection takes place at rate λsi . In particular, this rate is non-null if and only if $si \geq 1$, so we can restrict the study to the set of transient states $\Omega(n) = \{(s, i) \in \bar{\Omega}(n) : i \geq 1\}$. Let $\zeta_{n,\lambda,\gamma}(t)$ be the average infection rate in a population of composition $X_{n,\lambda,\gamma}(t)$, conditionally on $X_{n,\lambda,\gamma}(0) = x_0^n$. It is clear that, by definition,

$$\zeta_{n,\lambda,\gamma}(t) = \sum_{(s,i) \in \Omega(n)} \lambda si \mathbb{P}_{x_0^n}(X_t = (s, i)). \quad (4.3)$$

Consider $Q_{\lambda,\gamma}(n)$ the restriction of the generator of $X_{n,\lambda,\gamma}$ to $\Omega(n)$, which is defined as the following matrix indexed by states in $\Omega(n)$ ¹

$$\forall (s, i), (s', i') \in \Omega(n), \quad (Q_{\lambda,\gamma}(n))_{(s,i),(s',i')} = \begin{cases} -\lambda si - \gamma i & \text{if } (s', i') = (s, i); \\ \lambda si & \text{if } (s', i') = (s-1, i+1); \\ \gamma i & \text{if } (s', i') = (s, i-1); \\ 0 & \text{otherwise.} \end{cases} \quad (4.4)$$

Then it is well known that for all (s, i) in $\Omega(n)$,

$$\mathbb{P}_{x_0^n}(X_{n,\lambda,\gamma}(t) = (s, i)) = \left(e^{tQ_{\lambda,\gamma}(n)} \right)_{x_0^n, (s,i)}.$$

Thus, a computation readily yields the following Laplace transform, where $I_{d(n)}$ is the identity matrix of appropriate dimension, namely $d(n) = \#\Omega(n) = n(n+1)/2$: for any $u \geq 0$,

$$\mathfrak{L}_{n,\lambda,\gamma}(u) := \mathfrak{L}(\zeta_{n,\lambda,\gamma})(u) = \sum_{(s,i) \in \Omega(n)} \lambda si \left((uI_{d(n)} - Q_{\lambda,\gamma}(n))^{-1} \right)_{x_0^n, (s,i)}. \quad (4.5)$$

As we will see in the following proposition, we show that it is possible to go one step further and give an analytic expression for the relevant coefficients of

$$\widehat{Q}_{n,\lambda,\gamma}(u) := (uI_{d(n)} - Q_{\lambda,\gamma}(n))^{-1},$$

for any population size n . This allows us to give a more explicit expression of $\mathfrak{L}_{n,\lambda,\gamma}$.

We introduce the set

$$\mathcal{I}_n(k, m, i) = \left\{ (i_0, \dots, i_{m+1}) \in \{k\} \times \mathbb{N}^m \times \{i\} : i_m \leq i, \right. \\ \left. i_{j-1} - 1 \leq i_j \leq n - j \quad \forall 1 \leq j \leq m \right\}. \quad (4.6)$$

Proposition 4.1. *Let $k \in \{1, \dots, n\}$ and consider $(s, i) \in \Omega(n)$ such that $s \leq n - k$. Then for any $u \geq 0$,*

$$\left(\widehat{Q}_{n,\lambda,\gamma}(u) \right)_{(n-k,k),(s,i)} = \frac{1}{u + \lambda si + \gamma i} \sum_{i \in \mathcal{I}_n(k,m,i)} \prod_{j=0}^m q_{n,\lambda,\gamma}(\mathbf{i}, j; u) g_{n,m,\lambda,\gamma}(\mathbf{i}, j; u) \quad (4.7)$$

where $m = n - (s + i)$ and

$$q_{n,\lambda,\gamma}(\mathbf{i}, j; u) = \prod_{w=i_j}^{i_{j+1}-1} \left[1 + \frac{u + \gamma w}{\lambda(n - j - w)w} \right]^{-1} \quad (4.8)$$

and

$$g_{n,m,\lambda,\gamma}(\mathbf{i}, j; u) = \begin{cases} \left[1 + \frac{u + \lambda(n - j - i_{j+1} - 1)(i_{j+1} + 1)}{\gamma(i_{j+1} + 1)} \right]^{-1} & \text{for } j < m, \\ 1 & \text{for } j = m. \end{cases} \quad (4.9)$$

Furthermore, for every state $(s, i) \in \Omega(n)$ such that $s > n - k$, $\left(\widehat{Q}_{n,\lambda,\gamma}(u) \right)_{(n-k,k),(s,i)} = 0$.

¹We have made a slight change here compared to [26] since the mortality matrix Δ needed to be deleted from the expression of Q .

The proof of Proposition 4.1 uses simple arguments of linear algebra. Details can be found in Appendix 6.3. Using Equation (4.5), a more explicit expression of $\mathfrak{L}_{n,\lambda,\gamma}$ follows from equation (4.7). Let us define the ensemble

$$\begin{aligned} \mathcal{I}_n(m) = \{ & (i_0, i_1, \dots, i_m, i_{m+1}) \in \{1\} \times \mathbb{N}^{m+1} : i_{m+1} \leq n - m, \\ & i_m \leq i_{m+1}, \\ & i_{j-1} - 1 \leq i_j \leq n - j \quad \forall 1 \leq j \leq m\}. \end{aligned}$$

We can now state the result, using the same notations as in proposition 4.1.

Corollary 4.2. *For any integer n and any set of parameters $\lambda, \gamma > 0$ and any $u \geq 0$,*

$$\mathfrak{L}_{n,\lambda,\gamma}(u) = \sum_{m=0}^{n-1} \sum_{\mathbf{i} \in \mathcal{I}_n(m)} c_{n,\lambda,\gamma}(\mathbf{i}; u) \prod_{j=0}^m q_{n,\lambda,\gamma}(\mathbf{i}, j; u) g_{n,m,\lambda,\gamma}(\mathbf{i}, j; u) \quad (4.10)$$

with

$$c_{n,\lambda,\gamma}(\mathbf{i}; u) = \left[1 + \frac{u + \gamma i_{m+1}}{\lambda(n - m - i_{m+1})i_{m+1}} \right]^{-1}. \quad (4.11)$$

In the following section, we will see how $\mathfrak{L}_{n,\lambda,\gamma}$ intervenes in the computation of the growth rate r of the epidemic. Another quantity of similar nature will be needed, namely the Laplace transform $\mathfrak{G}_{n,\lambda,\gamma,\beta_G}$ of the average rate $\zeta_{n,\lambda,\gamma,\beta_G}^G$ at which all individuals of a structure of composition $X_{n,\lambda,\gamma}(t)$, conditionally on $X_{n,\lambda,\gamma}(0) = x_0^n$, contaminate individuals in the general population. Obviously, when the structure is in state $(s, i) \in \bar{\Omega}(n)$, this rate is given by $\beta_G i$, considering that the global proportion of susceptible individuals is close to one. In other words,

$$\mathfrak{G}_{n,\lambda,\gamma,\beta_G}(u) := \mathfrak{L}(\zeta_{n,\lambda,\gamma,\beta_G}^G)(u) = \sum_{(s,i) \in \Omega(n)} \beta_G i \left(\widehat{Q}_{n,\lambda,\gamma}(u) \right)_{x_0^n, (s,i)}. \quad (4.12)$$

This rate is positive if and only if $(s, i) \in \Omega(n)$. Proceeding like before, we obtain the following formula:

Corollary 4.3. *For any integer n , for any set of parameters $\lambda, \gamma, \beta_G > 0$, for any $u \geq 0$,*

$$\mathfrak{G}_{n,\lambda,\gamma,\beta_G}(u) = \sum_{m=0}^{n-1} \sum_{\mathbf{i} \in \mathcal{I}_n(m)} c'_{n,\lambda,\gamma,\beta_G}(\mathbf{i}; u) \prod_{j=0}^m q_{n,\lambda,\gamma}(\mathbf{i}, j; u) g_{n,m,\lambda,\gamma}(\mathbf{i}, j; u) \quad (4.13)$$

with

$$c'_{n,\lambda,\gamma,\beta_G}(\mathbf{i}; u) = \frac{\beta i_{m+1}}{u + \lambda(n - m - i_{m+1})i_{m+1} + \gamma i_{m+1}}. \quad (4.14)$$

Proof of Corollaries 4.2 and 4.3. Start by noticing that

$$\Omega(n) = \bigsqcup_{m=0}^{n-1} \bigsqcup_{i=1}^{n-m} \{(n - m - i, i)\}. \quad (4.15)$$

Thus, equation (4.5) becomes, using Proposition 4.1:

$$\mathfrak{L}_{n,\lambda,\gamma}(u) = \sum_{m=0}^{n-1} \sum_{i=1}^{n-m} \frac{\lambda(n - m - i)i}{u + \lambda(n - m - i)i + \gamma i} \sum_{\mathbf{i} \in \mathcal{I}_n(1,m,i)} \prod_{j=0}^m q_{n,\lambda,\gamma}(\mathbf{i}, j; u) g_{n,m,\lambda,\gamma}(\mathbf{i}, j; u) \quad (4.16)$$

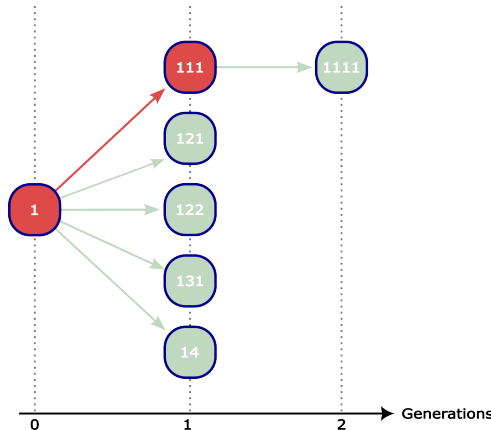


Figure 4.1: Illustration of the two-type household epidemic process. The example is the same as in Figure 3.1. The generations correspond here to generations of infected households, where the labels denote the first infected member of each household consistently with Figure 3.1. The colors of the arrows and of the households represent the type of infection, either globally (red) or locally (light green).

and the conclusion follows by the definition of $\mathcal{I}_n(m)$ and $c_{n,\lambda,\gamma}(\mathbf{i}; u)$. Similarly,

$$\mathfrak{G}_{n,\lambda,\gamma,\beta_G}(u) = \sum_{m=0}^{n-1} \sum_{i=1}^{n-m} \frac{\beta_G i}{u + \lambda(n-m-i)i + \gamma i} \sum_{\mathbf{i} \in \mathcal{I}_n(1,m,i)} \prod_{j=0}^m q_{n,\lambda,\gamma}(\mathbf{i}, j; u) g_{n,m,\lambda,\gamma}(\mathbf{i}, j; u) \quad (4.17)$$

and one concludes using the definition of $\mathcal{I}_n(m)$ and $c'_{n,\lambda,\gamma,\beta_G}$. \blacksquare

We now have introduced all necessary ingredients allowing for the computation of r , which is covered in detail in the next section.

4.2 Characterization of the initial growth rate

Let us now turn to the characterization of r for the multi-level model, which has been obtained by Pellis *et al.* [26]. We summarize their arguments for the sake of completeness and in order to illustrate how Corollaries 4.2 and 4.3 complement their approach.

Their main idea for computing the real time growth rate consists in considering the epidemic at the level of households instead of the individual level. Indeed, it is possible to reduce the epidemic dynamics to a two-type process, distinguishing households that have been contaminated *locally* (type L), if the first infected of the household contracted the disease at his workplace, or *globally* (type G) otherwise. Remember that, during the early phase of an epidemic, every newly contaminated household or workplace will be fully susceptible except for its member who has just been infected. Thus, a household infects another household *globally* whenever one of its contaminated members transmits the disease through the general population. Local transmission, on the other hand, occurs in the following way. Every time a member of a contaminated household H_1 is infected during its within-household epidemic, a within-workplace epidemic is started at his workplace. Then again, each coworker who is infected during the within-workplace epidemic introduces the disease into his household, which is regarded as *locally* contaminated by household H_1 . A slight subtlety is worth noticing: whether the first infected individual of a household participates in locally contaminating other households depends on the way he has been infected. If he has contracted the disease at his workplace, then he is not hold responsible for the the within-workplace epidemic there, and thus the other households that are infected

through his workplace are not considered locally infected by his household. However, the opposite happens if he was infected through the general population, because he then launches a new within-workplace epidemic. This two-type process is depicted in Figure 4.1.

Suppose now that the epidemic is in its exponential growth phase, meaning that there exists a growth rate r such that the number of infected individuals at time t is proportional to e^{rt} . Pellis *et al.* [26] argue that in this case, the household epidemic also grows exponentially at the same rate r . It thus is enough to study the previously introduced two-type process.

For $k, \ell \in \{L, G\}$, let $\zeta_{k\ell}(t)$ denote the average rate at which a household of type ℓ which was infected t units of time ago contaminates other households either locally if $k = L$, or globally if $k = G$. For $u \geq 0$, consider the matrix

$$K(u) = \begin{pmatrix} \mathfrak{L}\zeta_{GL}(u) & \mathfrak{L}\zeta_{GG}(u) \\ \mathfrak{L}\zeta_{LL}(u) & \mathfrak{L}\zeta_{LG}(u) \end{pmatrix}. \quad (4.18)$$

It is a classical result [14, 26] that for this two-type setting, the growth rate r is characterized as being the unique solution of the implicit equation

$$\rho(K(r)) = \frac{1}{2} \left(\text{Tr}(K(r)) + \sqrt{\text{Tr}(K(r))^2 - 4 \det(K(r))} \right) = 1, \quad (4.19)$$

where the operators ρ , Tr and \det denote the spectral radius, trace and determinant, respectively.

It thus only remains to take a closer look at $\zeta_{k\ell}(t)$ for all $k, \ell \in \{L, G\}$. As these are average rates of infection, one has to take into account the probability for a newly infected individual to belong to a household or workplace of a given size. Naturally, as households and workplaces are chosen independently uniformly at random, size-biased distributions appear both in the case of global and local infections. This leads us to introduce the following notation. For any application $f : (n, x) \mapsto f_n(x)$ on $\mathbb{N} \times \mathbb{R}$ and measure ν on \mathbb{N} , $\nu(f_\bullet)$ defines the function on \mathbb{R} such that $\nu(f_\bullet) : x \mapsto \sum_n \nu(n) f_n(x)$.

Within a household of size n , by definition, the average rate at which global transmissions occur is $\zeta_{n, \lambda_H, \gamma, \beta_G}^G$. Since a newly locally or globally contaminated household is of size n with probability $\hat{\pi}_n^H$, it follows that

$$\zeta_{GG} = \zeta_{GL} = \hat{\pi}^H(\zeta_{n, \lambda_H, \gamma, \beta_G}^G). \quad (4.20)$$

On the other hand, within a globally contaminated household of size n , new cases appear at rate $\zeta_{n, \lambda_H, \gamma}$. Once infected, each of these individual transmits the disease to his coworkers on average at rate $\zeta_{m, \lambda_W, \gamma}$, where m is the appropriate workplace size. This also applies to the globally infected individual who launched the within-household epidemic. If the household is contaminated locally, the reasoning is the same, except that the initially infected member is not hold responsible for his workplace epidemic, as he is himself a secondary case only. As a consequence,

$$\begin{aligned} \zeta_{LG} &= \hat{\pi}^W(\zeta_{\bullet, \lambda_W, \gamma}) + \hat{\pi}^H(\zeta_{\bullet, \lambda_H, \gamma}) * \hat{\pi}^W(\zeta_{\bullet, \lambda_W, \gamma}) \\ \zeta_{LL} &= \hat{\pi}^H(\zeta_{\bullet, \lambda_H, \gamma}) * \hat{\pi}^W(\zeta_{\bullet, \lambda_W, \gamma}). \end{aligned} \quad (4.21)$$

Using standard properties of Laplace transforms, $K(u)$ thus admits the following expression as derived by Pellis *et al.* [26], where the coefficients can now be computed using Corollaries 4.2 and 4.3:

$$K(u) = \begin{pmatrix} \hat{\pi}^H(\mathfrak{G}_{\bullet, \lambda_H, \gamma, \beta_G})(u) & \hat{\pi}^H(\mathfrak{G}_{\bullet, \lambda_H, \gamma, \beta_G})(u) \\ \hat{\pi}^H(\mathfrak{L}_{\bullet, \lambda_H, \gamma})(u) \hat{\pi}^W(\mathfrak{L}_{\bullet, \lambda_W, \gamma})(u) & (1 + \hat{\pi}^H(\mathfrak{L}_{\bullet, \lambda_H, \gamma})(u)) \hat{\pi}^W(\mathfrak{L}_{\bullet, \lambda_W, \gamma})(u) \end{pmatrix}. \quad (4.22)$$

Numerical methods then allow to solve the implicit equation (4.19) for the exponential growth rate r . We refer to Appendix 6.6 for details on the computation procedure.

4.3 ODE reduction of the multilevel model based on the initial growth rate

The reduced model is a standard deterministic *SIR* model, with infection rate derived from the growth rate r , obtained from Equation (4.19). The reduction of the model is defined by the following set of ordinary differential equations:

$$\begin{cases} \frac{dS}{dt} = -(r + \gamma)SI \\ \frac{dI}{dt} = (r + \gamma)SI - \gamma I \\ \frac{dR}{dt} = \gamma I \end{cases} \quad (4.23)$$

The prediction accuracy of the structured model by the reduced model is illustrated in Figure 4.2, where 1% of individuals are initially infected. In this example, we compare simulated epidemics of the stochastic structured model with scenario 1 from Table 2 and reference household and workplace size distributions to the ODE reduction from Table 1. The reduced model, based on the initial growth of infected population, accurately predicts, as expected, the early stages of the epidemic. We note however, that the prediction accuracy decreases with time and that the epidemic peak and the final size are overestimated by the reduce model.

Further explorations, using all scenarios and exploratory workplace distributions A, indicate the same trends. Comparison of epidemic outcomes such as the epidemic peak and the final size, between simulations of the stochastic structured model and their reduced counterpart are presented in Figure 4.3. We observe that, regardless of the scenario, the peak size and final epidemic size are largely correlated between the reduced model and numerical simulations of the stochastic structured model. A slight tendency to overestimate the epidemic outcomes with the reduced model can also be noticed. However, Figures 4.3 (top) illustrate that the epidemic outcomes of the reduced model remain close to the simulations of the stochastic structured model, with differences from the exact model simulations of less than 5% of the total number of individuals with the reduced model. The overestimation is more visible concerning the final epidemic size. This figure also shows that the epidemic parameters influence the prediction quality with the reduced model. This figure also illustrates the effect of the values of r and p_G on the prediction of the final epidemic size with the reduced model. Higher values of r , combined with low value for p_G (or high p_W), such as in scenario 1 and 2, tend to decrease the prediction accuracy with the reduced model. For lower values of the growth rate, which also corresponds to lower epidemic final size, the prediction accuracy is high, see for example scenarios 6 to 11.

The quality of the prediction is expected to be good for high values of p_G , as for $p_G = 1$ the reduced model is strictly equivalent to the deterministic approximation of the stochastic *SIR* model without structures. As the value of p_G decreases, propagation of the epidemic through households and workplaces becomes dominant and the structured model cannot be approximated by a uniformly mixing deterministic *SIR* model regardless of the growth rate, as illustrated in Figure 4.3 (bottom). This figure shows that the epidemic outcomes for the stochastic structured model cannot be obtained by any deterministic *SIR* model for scenarios with lower values of p_G such as scenario 1 and 2, which deviate from the black line representing the possible outcomes with a deterministic *SIR* model. In addition, Figure 4.3 (top) shows that, for scenarios with lower epidemic size, the prediction of epidemic outcomes by the reduced model is more accurate. This figure also illustrates that the peak size is accurately predicted by the reduced model in these cases, while the prediction of the final size is less accurate. This provides further evidence that the reduction captures the early phase of the epidemic.

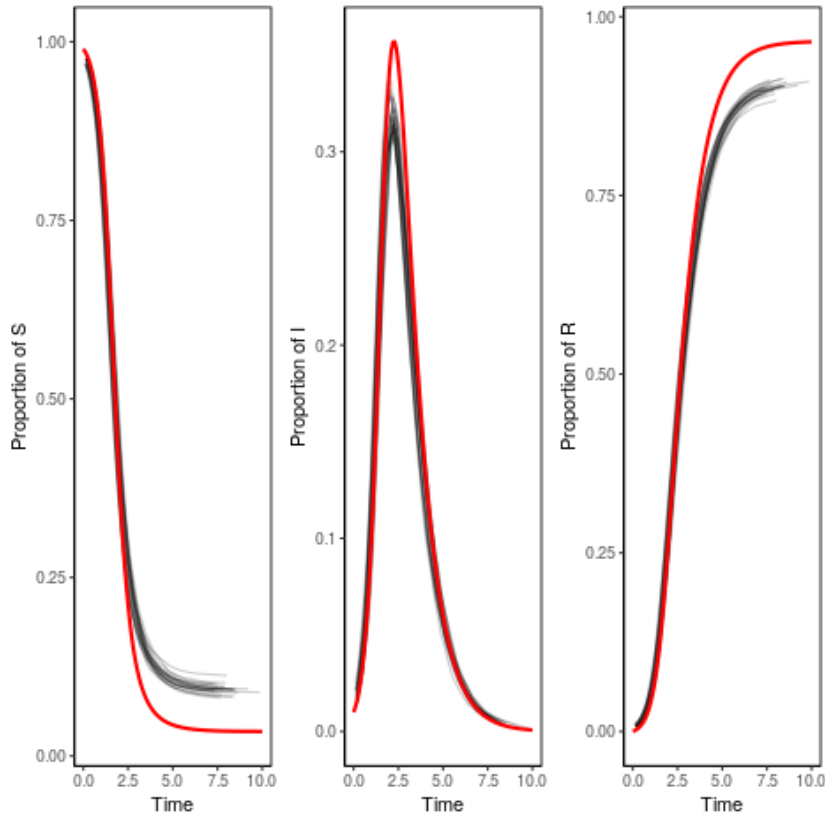


Figure 4.2: Evolution of the proportion of S, I, R individuals in 30 runs of the stochastic structured model (black), and the reduced model (red). Simulations are performed in a population with 100,000 individuals, with the reference household and workplace size distributions and epidemic parameters from scenario 1. The origin of time of the numerical simulation has been set to the time where 1% of individuals are infected. The simulation of the reduced model is performed with 1% of initially infected individuals.

4.4 Assessment of the reduction robustness

So far, in the modeling and for the simulations and computations, we have restricted ourselves to Markovian models and to the *SIR* structure. The Markovian assumption simplifies the parametrization: there is one single rate of infection for each of three infection ways and one single rate of recovery. This assumption is not necessary and most of our results can be formalized in more general contexts. Similarly, the *SIR* model is the canonical one, but models with different structures can be envisaged. We have checked by simulation that the reduction procedure based on the initial growth rate, as defined in Section 4.3, still provides good predictions in more general contexts. In Figure 6.8, we illustrate with an example the prediction of epidemic outcomes between the structured model with Gamma distributed individual recovery times and the corresponding reduced deterministic *SIR* model. We can make similar observations as for the Markovian model, that, generally speaking, the reduced model provides a good prediction of the epidemic outcomes. We also show with an example provided in Figure 6.9 that the reduction procedure provides good predictions of epidemic outcomes for an *SEIR* model, where an additional latent (and non infectious) *E* state is added to the *SIR* model. Details on the growth rate derivation for the *SEIR* model are provided in Section 6.2.

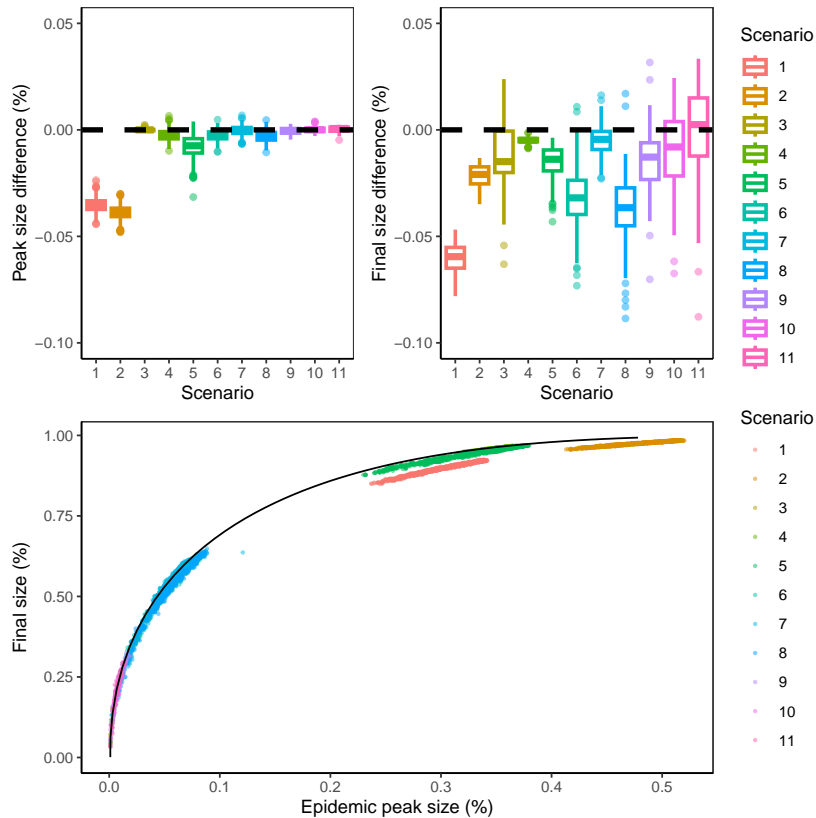


Figure 4.3: Boxplot of the differences in the peak sizes (top left) and final sizes (top right) between the complete and the reduced models, obtained from simulations of the stochastic structured model and the corresponding reduced model. Simulated final size as a function of the peak size is reported (bottom), the black line represents the value for the SIR model (4.23). Simulations of the stochastic structured model are performed with population size of 100,000, reference household distribution, workplace size distributions set A, for all scenarios from Table 2 (point color). Each combination of scenario and workplace size distribution from set A is repeated 10 times. Only simulations where an epidemic outbreak occurred (*i.e.* more than 3% of the population become infected) are reported in this figure.

5 Discussion

In this work, we study the effect of the size of closed structures (households, workplaces, schools...) on the propagation of epidemics, when individuals belong to different structures, chosen independently for a given individual. We assume that there is no dependence between the size of households and the size of workplaces. Our motivation comes in particular from the fact that control policies allow to change the distribution of structure sizes in various ways, for example by reducing the size of workplaces by teleworking or the size of schools by their (partial) closure. Optimizing control measures in terms of sanitary outcome has become a major challenge. Measuring the link between a social organisation, in terms of distribution of structure sizes, and the epidemic outcomes is a delicate issue. Indeed, explicit formula and low dimensional large population approximations are known only in uniformly mixing populations. These results concern explicit values for R_0 and initial growth rate r , simple equation for the total size of the outbreak, reduction to an SIR three dimensional ODE with two parameters. Formulae become more complex when considering one level of mixing (households) and even non explicitly tractable with an additional structure like workplaces, where the chain of transmission does not need mean field infection any longer to propagate.

We have both used existing approaches (namely [26]) and added new developments, by

providing more explicit expressions (Section 4) and simulations to study the role of structure sizes on the key outcomes of epidemics. Notice that even though the results of Corollaries 4.2 and 4.3 have not been used in this paper for evaluating the growth rate of simulation scenarios (details on computations in Appendix 6.5), their numerical implementation would have been an alternative method for achieving these computations. We have focused on the Markovian case, *i.e.* time of infection exponentially distributed and constant infection rate, and a simple *SIR* structure, with local infection rates proportional to the number of susceptible and infected individuals. This basic framework was complemented by a robustness study on more complex settings (Sections 3.4 and 4.4). According to our findings, the structure size distribution plays a role on the key outcomes in most scenarios. More precisely, for a given number of structures and a given number of individuals and thus for fixed average structure size, the way individuals are distributed has a quantitative impact on the growth rate of infections, the total number of infected individuals and the size of the infected peak. In this setting, the variance of the structures size distribution provides a good proxy of this impact.

This finding may be related to previously known results on the importance of the variance of the degree distribution in configuration model settings. Indeed, Britton *et al.* [10] have pointed out the impact of the degree distribution variance on the reproduction number for *SIR* epidemics on configuration graphs. Similarly, Ma *et al* [22] have studied the case of a model with two levels of mixing, corresponding to a layer of households and a general population taking the form of a configuration graph. They have shown that in this case, the variance of the degree distribution in the general population has a strong influence on epidemic dynamics. In the case of three layers of mixing, we can consider the epidemic at the household level. In this situation, the size distribution of the workplace plays a crucial role in determining the number of households to which a given household is directly connected. Although the framework is clearly more complex than a simple configuration model, the distribution of workplace size may play a role similar in spirit to that of the degree distribution in the previously mentioned models based on configuration graphs.

As for the limitations of our study, the robustness analyses that we have carried out (Sections 3.4 and 4.4), even if they are rather summary, point to robustness of the main results when certain assumptions are modified.

On the one hand, the effect of the structure size distribution may be overestimated by the fact that we consider a linear infection rate. Indeed, the rate at which a susceptible individual is infected at a given time is assumed to be proportional to the number of infected individuals at the same time. This probably overestimates the real infection rate. We consider here structures which form a partition of the population, with uniform mixing within each structure. We think this assumption is rather relevant for households but it could be improved and extended for workplaces (and schools), where different levels of mixing could be considered (services/departments within companies, classes within schools, etc). The simulation study with sub-linear infection rates in households and workplaces shows that the observation on the linear impact of variance on the final epidemic size is still valid (Figures 3.6 and 6.5). With sub-linear infection rates, we also observed similar results regarding the robustness of the prediction of epidemic outcomes using the reduced model, namely that the reduction is accurate for high values of p_G and a smaller epidemic size, see Figure 6.10. We note however, that the accuracy of the prediction using the reduced model is lower with sub-linear infection rates, and the early epidemic is not predicted as accurately. When it comes to policies and controls such as teleworking, a notion of effective size and/or effective infection rate should probably be introduced, which is one of the interesting perspectives.

On the other hand, the effect of the structure size distribution is observed when looking at the characteristics of the epidemic. Variance arises using the size biased law and the fact that mean final size of epidemics is comparable to the size structure. Furthermore, following preliminary

explorations, we observed that the dependence in the structure size distribution may imply a higher moment of it than the second moment linked to its variance. This could confer a greater impact of large structures than the variance would predict. This reinforces the importance of the structure size distribution and specifically the importance of the health benefit of moving toward structures (workplace offices, school classrooms...) of the same size. Variance remains the simplest proxy we have found in general, but further exploration may reveal another form of dependence.

Thus, based on our results, the variance of the structure size distribution, and more generally the ratio of the second to the first moment when the latter or the number of structures is not fixed, provides a good indicator to measure the impact of the distribution of individuals within small social structures. Nevertheless, much work remains to be done to identify the key parameters related to population structure that determine epidemic outcomes.

In this study, we are also interested in model reduction, in order to have a parsimonious model that is sufficiently accurate in terms of prediction and fast to run. This is an important issue, especially in a context where many scenarios and control policies need to be evaluated. Thus, our goal was to reduce the model to only a few parameters and variables. We obtained that by using the initial infection growth rate, which keeps track of the contact structure in a subtle (almost explicit but rather complex) way. We then make use of a classical *SIR* model (three variables and two parameters) as a reduction of the initial stochastic individual-centered model with three types of contacts.

In summary, our study highlights that knowledge and modeling of the size of contact structures appears to be important in characterizing the outcome of an epidemic. It also points to the major role of the initial growth rate of the infection, which is unique, contrary to R_0 which can have several interpretations in multilevel contact models, and also difficult to treat. We have tried to provide a more explicit expression for the initial growth rate, supplementing the literature. This allowed us first to conduct the study of the impact of the structure size distribution. As we already know, the initial growth rate provides the extinction/explosion criterion by its sign and the rate of progression. It is related to the peak and timing of the peak, when the epidemic dynamics explode, and to the extinction rate when this dynamics decline. The initial growth rate has also been a key input to the reduction problem, allowing a complex contact structure to be reduced to a few parameters, while retaining the essence of the qualitative and quantitative behavior of the epidemic beyond the initial time.

Acknowledgement. This work was partially funded by the Chair "Modélisation Mathématique et Biodiversité" of VEOLIA-Ecole Polytechnique-MNHN-F.X.

6 Appendix

6.1 Figures

6.2 Computation of the exponential growth rate for the *SEIR* model with two levels of mixing

In the *SEIR* model, subsequently to an infectious contact between an infected and a susceptible individual, the susceptible first becomes *exposed* (*E* state, assimilated to an infected but not yet infectious state) for a duration distributed according to an exponential law of parameter μ , before entering the infectious state. Thus, the computation of the exponential growth rate as proposed by Pellis *et al.* [26] needs to be adapted.

For a population of size n , consider the Markov chain giving the numbers $(S_t, E_t, I_t)_{t \geq 0}$ of susceptible, exposed and infected individuals in the population at time $t \geq 0$ after the beginning

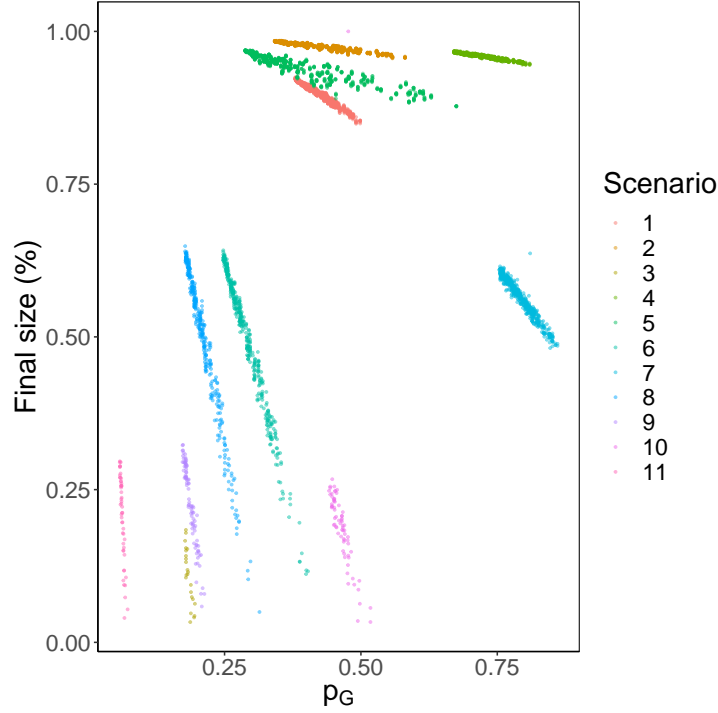


Figure 6.1: Simulated values of the final size as a function of the proportion of infection via global mixing (p_G) for all scenarios of Table 2 and all exploratory workplace size distributions from set A, Table 1. For each epidemic scenario and each workplace size distribution, simulations were repeated 10 times. Each coloured scatter plot on the figure thus contains 160×10 points. The household size distribution is the reference household size distribution.

of the epidemic, of transition rates

Transition	Rate	
$(s, e, i) \rightarrow (s - 1, e + 1, i)$	λsi ;	(6.1)
$(s, e, i) \rightarrow (s, e - 1, i + 1)$	μe ;	
$(s, e, i) \rightarrow (s, e, i - 1)$	γi .	

The set of transient states is then given by

$$\Omega'(n) = \{(s, e, i) \in (\mathbb{N} \cup 0)^3 : s + e + i \leq n, e + i \geq 1\},$$

of cardinal $d'(n) = n(n + 1)(n + 5)/6$. The restriction of the generator of this Markov chain to $\Omega(n)$ is given by $Q'_{\lambda, \gamma, \mu}(n)$ defined by: $\forall (s, e, i), (s', e', i') \in \Omega'(n)$,

$$(Q'_{\lambda, \gamma, \mu}(n))_{(s, e, i), (s', e', i')} = \begin{cases} -\lambda si - \mu e - \gamma i & \text{if } (s', e', i') = (s, e, i); \\ \lambda si & \text{if } (s', e', i') = (s - 1, e + 1, i); \\ \mu e & \text{if } (s', e', i') = (s, e - 1, i + 1); \\ \gamma i & \text{if } (s', e', i') = (s, e, i - 1); \\ 0 & \text{otherwise.} \end{cases} \quad (6.2)$$

Following the work of Pellis *et al.* [26] and adopting the notations introduced in Section 4, one can then easily see that the exponential growth rate r' of the *SEIR* model with two levels

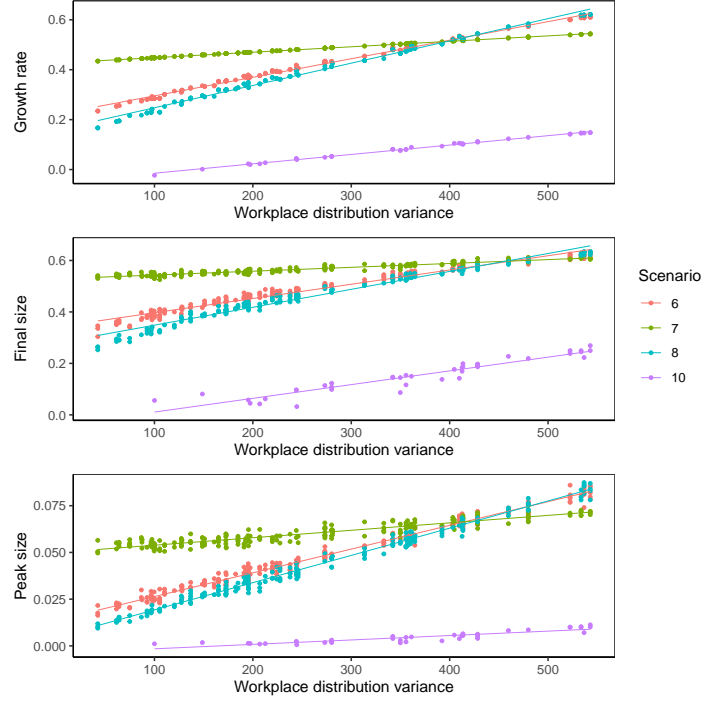


Figure 6.2: Influence of the variance of the workplace size distribution on the epidemic growth rate (top), final size (middle) and peak size (bottom). Simulations of the stochastic structured model with sub-linear infection rates in households and workplaces were performed with the reference household size distribution, exploratory workplace size distribution set B with average workplace size of 20 from Table 1 and epidemic scenarios 6, 7, 8 and 10 from Table 2. Simulations were repeated 10 times for each combination of scenario and workplace size distribution.

of mixing is characterized by the implicit equation

$$\rho(K'(r')) = 1, \quad (6.3)$$

where for $u \geq 0$,

$$K'(u) = \begin{pmatrix} \hat{\pi}^H \left(\mathfrak{G}'_{\bullet, \lambda_H, \mu, \gamma, \beta_G} \right) (u) & \hat{\pi}^H \left(\mathfrak{G}'_{\bullet, \lambda_H, \mu, \gamma, \beta_G} \right) (u) \\ \hat{\pi}^H \left(\mathfrak{L}'_{\bullet, \lambda_H, \mu, \gamma} \right) (u) \hat{\pi}^W \left(\mathfrak{L}'_{\bullet, \lambda_W, \mu, \gamma} \right) (u) & \left(1 + \hat{\pi}^H \left(\mathfrak{L}'_{\bullet, \lambda_H, \mu, \gamma} \right) (u) \right) \hat{\pi}^W \left(\mathfrak{L}'_{\bullet, \lambda_W, \mu, \gamma} \right) (u) \end{pmatrix}, \quad (6.4)$$

given the definition for $\beta, \lambda, \mu, \gamma > 0$ of

$$\begin{aligned} \mathfrak{G}'_{\bullet, \lambda, \mu, \gamma, \beta}(u) &= \sum_{(s, e, i) \in \Omega'(n)} \beta i \left((u I_{d'}(n) - Q'_{\lambda, \gamma, \mu}(n))^{-1} \right)_{(n-1, 1, 0), (s, e, i)}, \\ \mathfrak{L}'_{\bullet, \lambda, \mu, \gamma}(u) &= \sum_{(s, e, i) \in \Omega'(n)} (\lambda s i + \mu e) \left((u I_{d'}(n) - Q'_{\lambda, \gamma, \mu}(n))^{-1} \right)_{(n-1, 1, 0), (s, e, i)}. \end{aligned} \quad (6.5)$$

6.3 Proof of proposition 4.1

The notations are the same as previously introduced in Section 4.1. We further let I_k denote the identity matrix of dimension k , and $M_{n, m}(\mathbb{R})$ (resp. $M_n(\mathbb{R})$) the space of $n \times m$ (resp. $n \times n$) matrices with real coefficients. The aim is to compute

$$\hat{Q}_{n, \lambda, \gamma}(u) = (u I_{d(n)} - Q_{\lambda, \gamma}(n))^{-1} \quad (6.6)$$

for $u \geq 0$, which allows us to obtain Corollaries 4.2 and 4.3.

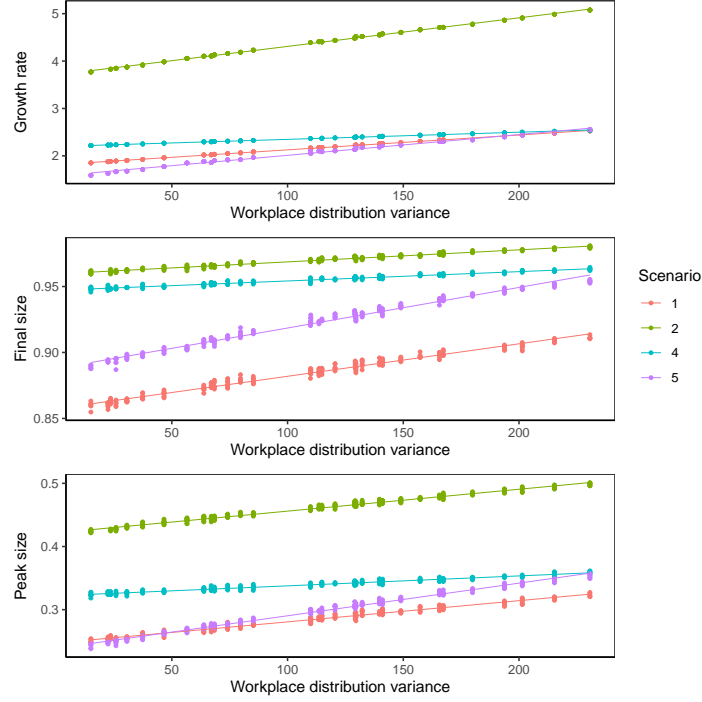


Figure 6.3: Influence of the variance of the workplace size distribution on the epidemic growth rate (top), final size (middle) and peak size (bottom). Simulations of the stochastic structured model with linear infection rates in households and workplaces were performed with the reference household size distribution, exploratory workplace size distribution set C with average workplace size of 7 from Table 1 and epidemic scenarios 1, 2, 4 and 5 from Table 2. Simulations were repeated 10 times for each combination of scenario and workplace size distribution.

Proof of proposition 4.1. We start by noticing that when $n = 1$, necessarily, $k = 1$, $(s, i) = (0, 1)$ and $m = 0$. The set of interest becomes $\mathcal{I}_1(1, 0, 1) = \{(1, 1)\}$, and the right side of equation (4.7) equals $(u + \gamma)^{-1}$. On the other hand, it is obvious that $(uI_1 - Q_{\lambda, \gamma}(1)) = (u + \gamma)$. Thus, (4.7) holds when $n = 1$.

Suppose now that equation (4.7) is true for some integer n . We proceed by induction. Notice that it is possible to enumerate the states of $\Omega(n + 1)$ in such a way that $Q_{\lambda, \gamma}(n + 1)$ is upper triangular. Indeed, it is enough to enumerate first all states in $\widehat{\Omega}(n + 1) = \{(s, i) \in \Omega(n + 1) : s + i = n + 1\}$ as $\{(n + 1 - k, k) : 1 \leq k \leq n + 1\}$, so that progression from one state to another occurs by infections which are not reversible as individuals are immune after infection. This process is repeated for states $\widehat{\Omega}(m) = \{(m - k, k) : 1 \leq k \leq m\}$ for $m = n, \dots, 1$, so that transition from one set of states to the next occurs by removal of an infected, which also is irreversible as individuals will remain immune afterwards.

This way of enumerating $\Omega(n + 1)$ is particularly interesting as obviously, $\Omega(n + 1) = \bigsqcup_{m=1}^{n+1} \widehat{\Omega}(m)$, so that $Q_{\lambda, \gamma}(n + 1)$ can be regarded as the following block matrix:

$$Q_{\lambda, \gamma}(n + 1) = \begin{pmatrix} A & B \\ 0 & Q_{\lambda, \gamma}(n) \end{pmatrix}. \quad (6.7)$$

Here, blocks $A \in M_{n+1}(\mathbb{R})$ and $B \in M_{n+1, d(n)}(\mathbb{R})$ represent events of infections and removals in $\widehat{\Omega}(n + 1)$, respectively. As previously, the elements of $Q_{\lambda, \gamma}(n + 1)$ can also be indexed by states in $\Omega(n + 1)$. Naturally, $uI_{d(n+1)} - Q_{\lambda, \gamma}(n + 1)$ also is a block matrix, simply replacing the blocks A and $Q_{\lambda, \gamma}(n)$ by $A' = uI_{n+1} - A$ and $uI_{d(n)} - Q_{\lambda, \gamma}(n)$ respectively.

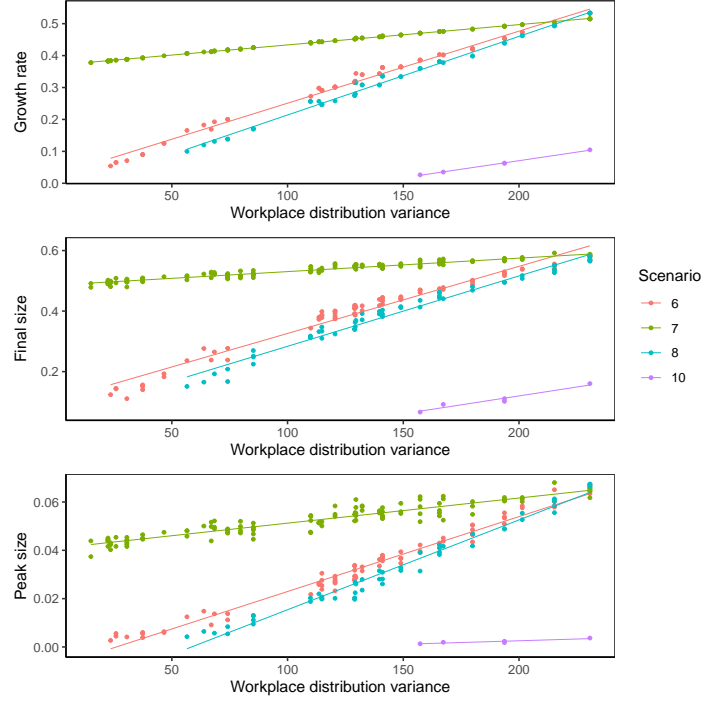


Figure 6.4: Influence of the variance of the workplace size distribution on the epidemic growth rate (top), final size (middle) and peak size (bottom). Simulations of the stochastic structured model with linear infection rates in households and workplaces were performed with the reference household size distribution, exploratory workplace size distribution set C with average workplace size of 7 from Table 1 and epidemic scenarios 6, 7, 8 and 10 from Table 2. Simulations were repeated 10 times for each combination of scenario and workplace size distribution.

More precisely, A' is an upper bidiagonal matrix such that

$$\begin{aligned} \forall k \in \{1, \dots, n+1\}, \quad A'_{k,k} &= A'_{(n+1-k,k),(n+1-k,k)} = u + \lambda(n+1-k)k + \gamma k, \\ \forall k \in \{1, \dots, n\}, \quad A'_{k,k+1} &= A'_{(n+1-k,k),(n+1-(k+1),k+1)} = -\lambda(n+1-k)k. \end{aligned} \quad (6.8)$$

Since A is upper diagonal, its inverse matrix is easily computable [11], and letting $a_{k,i}^{(n+1)} = (A')_{(n+1-k,k),(n+1-i,i)}^{-1}$, we have:

$$a_{k,i}^{(n+1)} = \mathbf{1}_{i \geq k} \frac{1}{u + \lambda(n+1-i)i + \gamma i} \prod_{j=k}^{i-1} \left(1 + \frac{u + \gamma j}{\lambda(n+1-j)j} \right)^{-1}. \quad (6.9)$$

Furthermore, as the only states of $\Omega(n)$ that are directly accessible by removal from $\widehat{\Omega}(n+1)$ belong to $\widehat{\Omega}(n)$, all coefficients of B are null except for the following:

$$B_{k,k-1} = B_{(n+1-k,k),(n+1-k,k-1)} = -\gamma k, \quad \forall k \in \{2, \dots, n+1\}. \quad (6.10)$$

Using the fact that $uI_{d(n+1)} - Q_{\lambda,\gamma}(n+1)$ is a block matrix and that A' and $uI_{d(n)} - Q_{\lambda,\gamma}(n)$ are upper triangular with positive diagonal coefficients and thus invertible, we have the following:

$$\widehat{Q}_{n+1,\lambda,\gamma}(u) = (uI_{d(n+1)} - Q_{\lambda,\gamma}(n+1))^{-1} = \begin{pmatrix} (A')^{-1} & -(A')^{-1}B\widehat{Q}_{n,\lambda,\gamma}(u) \\ 0 & \widehat{Q}_{n,\lambda,\gamma}(u) \end{pmatrix}. \quad (6.11)$$

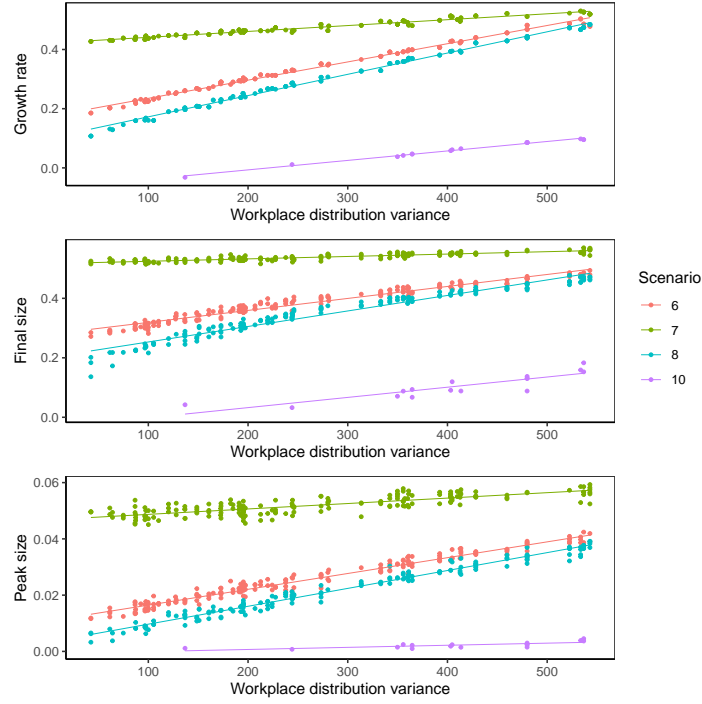


Figure 6.5: Influence of the variance of the workplace size distribution on the epidemic growth rate (top), final size (middle) and peak size (bottom). Simulations of the stochastic structured model with sub-linear infection rates in households and workplaces were performed with the reference household size distribution, exploratory workplace size distribution set B with average workplace size of 20 from Table 1 and epidemic scenarios 6, 7, 8 and 10 from Table 2. Simulations were repeated 10 times for each combination of scenario and workplace size distribution.

Thus, we obtain that, for all $k, i \in \{1, \dots, n+1\}$ and $(s, i) \in \Omega(n)$,

$$\begin{aligned} \left(\widehat{Q}_{n+1, \lambda, \gamma}(u)\right)_{(n+1-k, k), (n+1-i, i)} &= a_{k, i}^{(n+1)}; \\ \left(\widehat{Q}_{n+1, \lambda, \gamma}(u)\right)_{(n+1-k, k), (s, i)} &= \sum_{w=2}^{n+1} a_{k, w}^{(n+1)} \gamma w \left(\widehat{Q}_{n, \lambda, \gamma}(u)\right)_{(n+1-w, w-1), (s, i)}. \end{aligned} \quad (6.12)$$

Let us turn to proving that equation (4.7) holds true for $n+1$. Let $k \in \{1, \dots, n+1\}$ and consider $(s, i) \in \Omega(n+1)$ such that $s \leq (n+1) - k$ and define $m = (n+1) - (s+i)$.

Notice that $m = 0$ if and only if $(s, i) \in \widehat{\Omega}(n+1)$ and $s = n+1 - i$. As a consequence, if $i < k$, the set $\mathcal{I}_{n+1}(k, 0, i)$ is empty; otherwise, if $i \geq k$, $\mathcal{I}_{n+1}(k, 0, i) = \{(k, i)\}$. In both cases, the right hand side of equation (4.7) equals $a_{k, i}^{(n+1)}$. Thus, by Equation (6.12), Assertion (4.7) follows.

Consider now the case $m > 0$, *i.e.* $(s, i) \in \Omega(n)$. It follows from Equation (6.12), using the change of variable $k' = w - 1$, that

$$\left(\widehat{Q}_{n+1, \lambda, \gamma}(u)\right)_{(n+1-k, k), (s, i)} = \sum_{k'=1}^n a_{k, k'+1}^{(n+1)} \gamma (k'+1) \left(\widehat{Q}_{n, \lambda, \gamma}(u)\right)_{(n-k', k'), (s, i)}. \quad (6.13)$$

Using the inductive hypothesis and noticing that $n - (s+i) = m - 1$, we get that for any $k' \in \{1, \dots, n\}$,

$$\left(\widehat{Q}_{n, \lambda, \gamma}(u)\right)_{(n-k', k'), (s, i)} = \frac{1}{u + \lambda s i + \gamma i} \sum_{i \in \mathcal{I}_n(k', m-1, i)} \prod_{j=1}^m q_{n, \lambda, \gamma}(i, j-1; u) g_{n, m-1, \lambda, \gamma}(i, j-1; u).$$

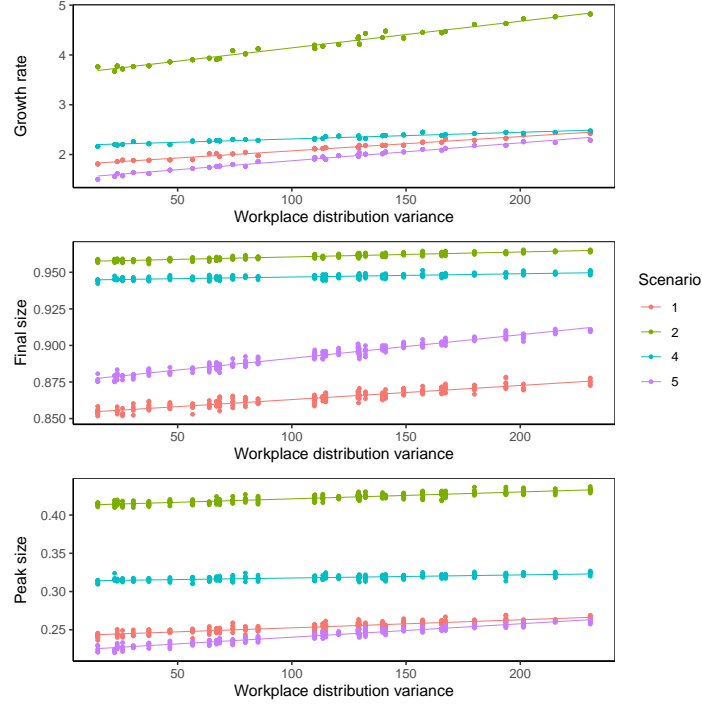


Figure 6.6: Influence of the variance of the workplace size distribution on the epidemic growth rate (top), final size (middle) and peak size (bottom). Simulations of the stochastic structured model with sub-linear infection rates in households and workplaces were performed with the reference household size distribution, exploratory workplace size distribution set C with average workplace size of 7 from Table 1 and epidemic scenarios 1, 2, 4 and 5 from Table 2. Simulations were repeated 10 times for each combination of scenario and workplace size distribution.

Notice that if $\mathbf{i} \in \mathbb{N}^{m+2}$ is such that $i_{j-1} = i'_j$ for all j , then $q_{n,\lambda,\gamma}(\mathbf{i}, j-1; u) = q_{n+1,\lambda,\gamma}(\mathbf{i}', j; u)$ and $g_{n,m-1,\lambda,\gamma}(\mathbf{i}, j-1; u) = g_{n+1,m,\lambda,\gamma}(\mathbf{i}', j; u)$. Letting τ be the projection on \mathbb{N}^{m+2} : for any $\mathbf{i}' = (i'_0, \dots, i'_{m+1}) \in \mathbb{N}^{m+2}$, $\tau(\mathbf{i}') = (i_1, \dots, i_{m+1})$, we get that:

$$\sum_{\mathbf{i} \in \mathcal{I}_n(k', m-1, i)} \prod_{j=1}^m q_{n,\lambda,\gamma}(\mathbf{i}, j-1; u) g_{n,m-1,\lambda,\gamma}(\mathbf{i}, j-1; u) = \sum_{\substack{\mathbf{i}' \in \mathbb{N}^{m+2}: \\ \tau(\mathbf{i}') \in \mathcal{I}_n(k', m-1, i)}} \prod_{j=1}^m q_{n+1,\lambda,\gamma}(\mathbf{i}', j; u) g_{n+1,m,\lambda,\gamma}(\mathbf{i}', j; u). \quad (6.14)$$

Furthermore, for $\mathbf{i}' \in \mathbb{N}^{m+2}$ such that $i'_0 = k, i'_1 = k'$, it holds that

$$a_{k,k'+1}^{(n+1)} \gamma(k'+1) = \mathbf{1}_{\{k'+1 \geq k\}} q_{n+1,\lambda,\gamma}(\mathbf{i}', 0; u) g_{n+1,m,\lambda,\gamma}(\mathbf{i}', 0; u). \quad (6.15)$$

Thus, noticing that the limits of the sum over k' in equation (6.13) taken together with $\mathbf{1}_{\{k'+1 \geq k\}}$ from equation (6.15) induce that $k-1 \leq k' \leq n$, equation (6.13) yields the desired result:

$$\left(\widehat{Q}_{n+1,\lambda,\gamma}(u) \right)_{(n+1-k,k),(s,i)} = \frac{1}{u + \lambda s i + \gamma i} \sum_{\mathbf{i}' \in \mathcal{I}_{n+1}(k,m,i)} \prod_{j=0}^m q_{n+1,\lambda,\gamma}(\mathbf{i}', j; u) g_{n+1,\lambda,\gamma}(\mathbf{i}', j; u).$$

This completes the proof; ■

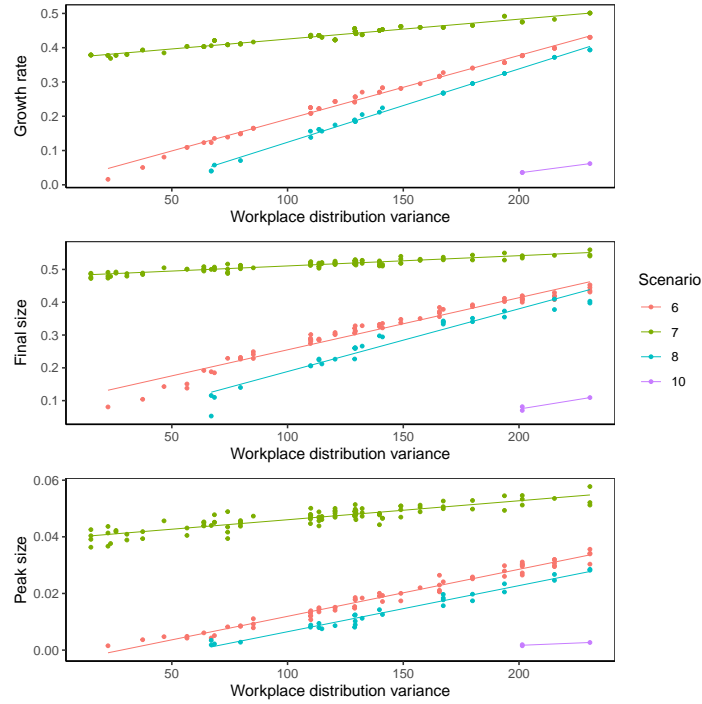


Figure 6.7: Influence of the variance of the workplace size distribution on the epidemic growth rate (top), final size (middle) and peak size (bottom). Simulations of the stochastic structured model with sub-linear infection rates in households and workplaces were performed with the reference household size distribution, exploratory workplace size distribution set C with average workplace size of 7 from Table 1 and epidemic scenarios 6, 7, 8 and 10 from Table 2. Simulations were repeated 10 times for each combination of scenario and workplace size distribution.

6.4 Reduction of the SEIR model with two levels of mixing, numerical aspects

The reduced model is a standard uniformly mixing deterministic *SEIR* model, with infectious contact rate $\hat{\lambda}$ and transition rate μ for the transition from *E* to *I*. As before, γ designates the recovery rate of infected individuals.

Notice that, given the parameters $\hat{\lambda}$, μ and γ , the epidemic growth rate of the deterministic *SEIR* model can be computed by solving equation (4.1) with $\zeta(\tau) = (\hat{\lambda}/\gamma)\omega(\tau)$, where $\omega(\tau)$ is the distribution of infection times for an infected individual in a uniformly mixed population and $\hat{\lambda}/\gamma$ is the average number of infections caused by an individual in early stages of the *SEIR* epidemic.

In order to choose the value of $\hat{\lambda}$ for the reduced model we proceed as follows. First, the epidemic growth rate r of the *SEIR* model with two layers of mixing is computed following section 6.2. It then remains to set $\hat{\lambda}$ in such a way that the epidemic growth rate of the deterministic *SEIR* model, which can be computed as described above, is equal to r .

The reduced model is then defined by the following set of ordinary differential equations:

$$\begin{cases} \frac{dS}{dt} = -\hat{\lambda}SI \\ \frac{dE}{dt} = \hat{\lambda}SI - \mu E \\ \frac{dI}{dt} = \mu E - \gamma I \\ \frac{dR}{dt} = \gamma I \end{cases} \quad (6.16)$$

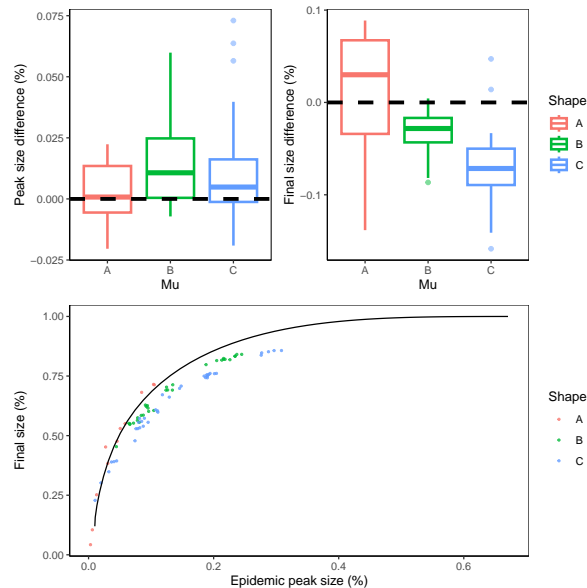


Figure 6.8: Boxplot of the differences in the peak sizes (top left) and final sizes (top right) between the complete *SIR* model with gamma distributed recovery rate and the reduced model defined in (4.23), obtained from simulations of the stochastic structured model and the corresponding reduced model. Simulated final size as a function of the peak size is reported (bottom), the black line represents the value for the *SIR* model. Simulations of the stochastic structured model are performed with population size of 10,000. Workplace and household sizes are set to 4. The recovery rate is set to 1 and three gamma distributions with mean value of 1 are considered for the recovery rate. The shape and rate parameters are equal and set to 1 (A), 3 (B) and 6 (C). Each point corresponds to different values of the infection parameters β_G , β_H and β_W . Only simulations where an epidemic outbreak occurred (*i.e.* more than 3% of the population become infected) are reported in this figure.

6.5 Parameter values for scenarios

The size distribution of households and workplaces combined with structure-dependent infection rates determines a value for the initial growth rate of the epidemic r , as well as probabilities of infections corresponding to the three sources, global mixing p_G , households p_H and workplaces p_W . Due to the constraints imposed by the structure size distributions in the structured epidemic model, it is not always possible to find numerical values of infection rates that lead to given values of growth rate r and infection probabilities p_G , p_H and p_W . Parameter selection for scenarios in Table 2 was performed, for the reference household and workplace distributions, using an optimisation procedure that yields infection rates leading to a solution for growth rate and infection probabilities values as close as possible to the target values. It relies on a cost function based on the mean square error between the target values and the trial values of r , p_G , p_H and p_W . A hyper-parameter α controls the importance given to the error on the growth rate. Scenario 1 was inspired by values reported in [16] and [17] for the SARS-Cov-2 epidemic. Other scenarios are designed by increasing or decreasing either the growth rate r or the infection probabilities. Scenarios provided in Table 2, combined with several workplace distributions from 1, allow the exploration of the relevant behavior of the structured epidemic model. The epidemic final size for each scenario and workplace distribution is reported in Figure 6.1.

6.6 Numerical computations of epidemic parameters and outcomes

The values of R_0 , p_G , p_H and p_W are obtained from Equations (3.2) and (3.3). They both require the values of \mathcal{I}_G , \mathcal{I}_H , \mathcal{I}_W which are given by Equation (3.1). Evaluations of \mathcal{I}_G , \mathcal{I}_H , \mathcal{I}_W require the values of $i_H(k)$ and $i_W(k)$ which we obtained from numerical simulations of the within

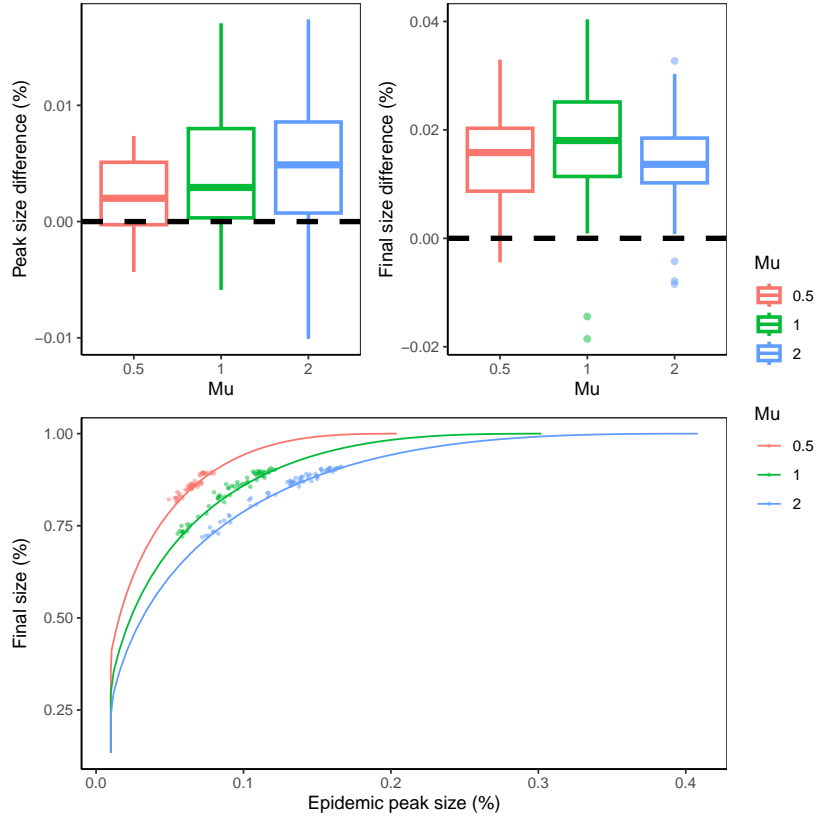


Figure 6.9: Boxplot of the differences in the peak sizes (top left) and final sizes (top right) between the complete and the reduced *SEIR* models, obtained from simulations of the stochastic structured model and the corresponding reduced model defined in (6.16). Simulated final size as a function of the peak size is reported (bottom), the lines represent the values for the *SEIR* model with corresponding value of μ . Simulations of the stochastic structured model are performed with population size of 10,000. Workplace and household sizes are set to 4. The recovery rate is set to 1 and three values of the transition rate μ are used (color). Each point corresponds to different values of the infection parameters β_G , β_H and β_W . Only simulations where an epidemic outbreak occurred (*i.e.* more than 3% of the population become infected) are reported in this figure.

structures epidemic. The growth rate r can be obtained in several ways, which all involve some form of solution for Equation (4.19), which we solved using a root finding algorithm. Elements of Matrix (4.18) can be obtained by numerical simulation of within structure epidemics, numerical integration and numerical matrix inversion. We also provide analytical formulations for the *SIR* and *SEIR* models, with linear infection rates, in Equations (4.5) and (6.5). Alternatively, we provide a fully analytical way to obtain the growth rate of the *SIR* model with linear infection rates, in Corollaries 4.2 and 4.3. The values of the epidemic peak and size are obtained by stochastic simulation of the structured model, and the values of the epidemic peak and size of the reduced model are obtained by simulation of Equation (4.23). For a summary of the numerical evaluation of epidemic quantities, see Table 3.

References

- [1] K. B. Athreya, P. E. Ney (2004). "Branching processes". Dover Publications, Inc., Mineola, NY.
- [2] A. Backhausz, I. Z. Kiss, P. L. Simon (2022). "The impact of spatial and social structure on an SIR epidemic on a weighted multilayer network". *Periodica Mathematica Hungarica*,

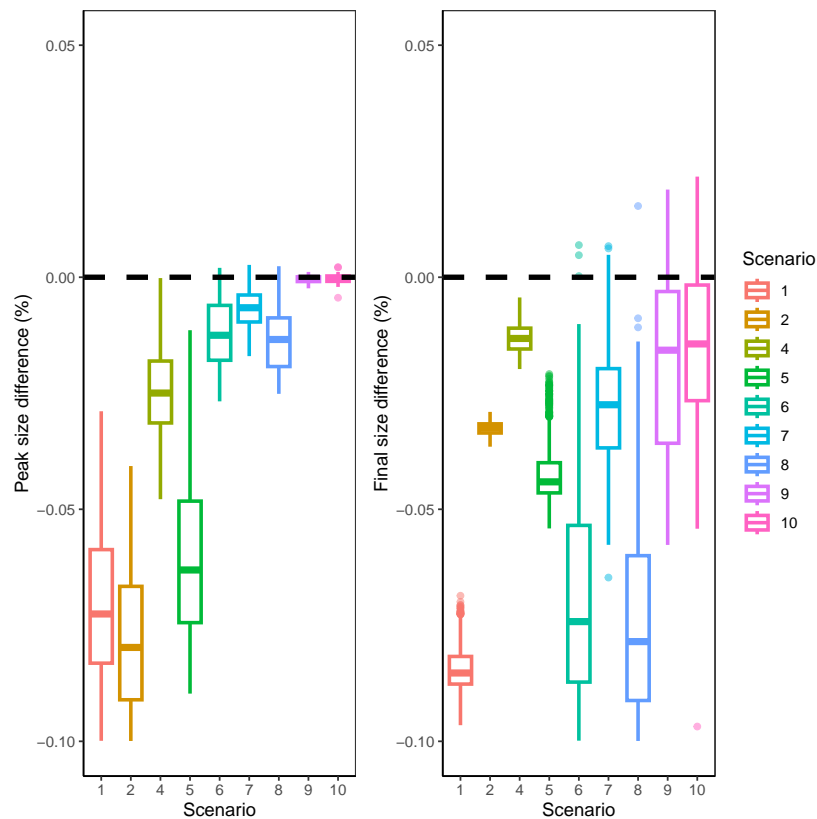


Figure 6.10: Boxplot of the differences in the peak sizes and (left) and final sizes (right) between the complete and the reduced models, obtained from simulations of the stochastic structured model with sub-linear rate and the corresponding reduced model. Simulations of the stochastic structured model are performed with population size of 100,000, reference household distribution, workplace size distributions set A, for all scenarios from Table 2 (point color). Each combination of scenario and workplace size distribution from set A is repeated 10 times. Only simulations where an epidemic outbreak occurred (*i.e.* more than 3% of the population become infected) are reported in this figure.

85:343-363.

- [3] F. Ball, D. Mollison, G. Scalia-Tomba (1997). "Epidemics with two levels of mixing". *Annals of Applied Probability* **7**:46-89.
- [4] F. Ball, P. Neal (2002). "A general model for stochastic SIR epidemics with two levels of mixing", *Mathematical Biosciences*, **180**:73-102.
- [5] F. Ball, L. Pellis, P. Trapman (2016). "Reproduction numbers for epidemic models with households and other social structures. II. Comparisons and implications for vaccination." *Mathematical Biosciences*, **274**:108-139.
- [6] F. Ball, P. Donnelly (1995). "Strong approximations for epidemic models." *Stochastic Processes and their Applications*, **55**:1-21.
- [7] F. Ball, D. Sirl (2014). "Epidemics on random intersection graphs". *The Annals of Applied Probability*, **24**(3):1081-1128.
- [8] A. D. Barbour, G. Reinert (2013). "Approximating the epidemic curve". *Electronic Journal of Probability*, **54**:1-30.

Epidemic parameter/outcome	Numerical method
$\mathcal{I}_G, \mathcal{I}_G, \mathcal{I}_W$	Equation (3.1), with $i_H(k)$ and $i_W(k)$ obtained from numerical simulations of the within structure epidemic.
R_0	Largest eigenvalue of Equation (3.2).
p_G, p_H and p_W	Equation (3.3).
Growth rate r	Equation (4.19) with Laplace transforms for elements of matrix (4.18) which can be numerically evaluated. Alternatively, in the case of the <i>SIR</i> (or <i>SEIR</i>) model with linear infection rates, these elements are defined in Equation (4.5) (resp. (6.5)), where matrices in the sum are inverted numerically.
Peak and final size	Numerical simulation of the structured epidemic model or numerical simulation of Equation (4.23) for the reduced epidemic model.

Table 3: Numerical methods used to compute epidemic parameters and outcomes.

- [9] A.D. Barbour, S. Utev (2004). "Approximating the Reed-Frost epidemic process". *Stochastic Processes and their Applications*, **113**:173-197
- [10] T. Britton, S. Janson and A. Martin-Löf (2007). "Graphs with specified degree distributions, simple epidemics, and local vaccination strategies". *Advances in Applied Probability*, **39**:922-948.
- [11] G. Chatterjee (1974). "Negative integral powers of a bidiagonal matrix". *Mathematics of Computation*, **28**:713-714.
- [12] N.G. Davies, P. Klepac, Y. Liu, K. Prem, M. Jit, CMMID COVID-19 working group, R. M. Eggo (2020). "Age-dependent effects in the transmission and control of COVID-19 epidemics". *Nature Medicine* **26**:1205-1211.
- [13] M. del Valle Rafo, J. P. Di Mauro, J. P. Aparicio (2021). "Disease dynamics and mean field models for clustered networks". *Journal of Theoretical Biology* **526**:110554.
- [14] O. Diekmann, J.A.P. Heesterbeek (2000). "Mathematical Epidemiology of Infectious Diseases: Model Building, Analysis and Interpretation". *Wiley series in mathematical and computational biology*. Wiley, Chichester.
- [15] S.N. Ethier, T.G. Kurtz (1986). *Markov processes, Characterization and Convergence*. John Wiley & Sons, New York.
- [16] S. Galmiche, T. Charmet, L. Schaeffer, J. Paireau, R. Grant, O. Cheny, C. Von Platen, C., A. Maurizot, C. Blanc, A. Dinis, S. Martin, F. Omar, C. David, A. Septfons, S. Cauchemez, F. Carrat, A. Mailles, D. Levy-Bruhl, A. Fontanet (2021). "Exposures associated with SARS-CoV-2 infection in France: A nationwide online case-control study". *The Lancet Regional Health-Europe* **7**:100148.
- [17] Galmiche, S., Charmet, T., Schaeffer, L., Grant, R., Fontanet, A., Paireau, J., ..., Levy-Bruhl, D. (2021). *Etude des facteurs sociodémographiques, comportements et pratiques associés à l'infection par le SARS-CoV-2 (ComCor)* (Doctoral dissertation, Institut Pasteur; Caisse Nationale d'Assurance Maladie; IPSOS; Institut Pierre Louis d'Epidémiologie et de Santé Publique (IPLESP); Santé Publique France).

- [18] J. R. Giles, E. zu Erbach-Schoenberg, A. J. Tatem, L. Gardner, O. N. Bjornstad, C. J. E. Metcalf, A. Wesolowski (2020). "The duration of travel impacts the spatial dynamics of infectious diseases". *Proceedings of the National Academy of Science* **117**:22572-22579.
- [19] E. Goldstein, K. Paur, C. Fraser, E. Kenah, J. Wallinga, M. Lipsitch (2009). "Reproductive numbers, epidemic spread and control in a community of households". *Mathematical Biosciences*, **221**:11-25.
- [20] T. House, M. Keeling (2008). "Deterministic epidemic models with explicit household structure". *Mathematical Biosciences*, **213**:29-39.
- [21] M. Keeling, K. Eames (2005). "Networks and epidemic models". *Journal of the Royal Society Interface*, **2**:295-307.
- [22] J. Ma, P. van den Driessche, F.H. Willeboordse (2013). "Effective degree household network disease model". *Journal of Mathematical Biology*, **66**:75-94.
- [23] A. Mendez-Brito, C. El Bcheraoui, F. Pozo-Martin (2021). "Systematic review of empirical studies comparing the effectiveness of non-pharmaceutical interventions against COVID-19". *Journal of Infection*, **83**:281-293
- [24] C.J. Mode (2000). "Life cycle models and mean functions", in *Stochastic processes in epidemiology: HIV/AIDS, other infectious diseases and computers*, World Scientific, pp 175-180.
- [25] L. Pellis, N. M. Ferguson, C. Fraser (2009). "Threshold parameters for a model of epidemic spread among households and workplaces". *Journal of the Royal Society Interface*, **6**: 979-987.
- [26] L. Pellis, N. M. Ferguson, C. Fraser (2011). "Epidemic growth rate and household reproduction number in communities of households, schools and workplaces". *Journal of Mathematical Biology*, **63**:691-734.
- [27] L. Pellis, F. Ball, P. Trapman (2012). "Reproduction numbers for epidemic models with households and other social structures. I. Definition and calculation of R_0 ". *Mathematical Biosciences*, **235**:85-97.
- [28] M. I. Simoy, J. P. Aparicio (2022). "Socially structured model for COVID-19 pandemic: design and evaluation of control measures". *Computational and Applied Mathematics*, **41**:14.
- [29] P. Trapman, F. Ball, J.-S. Dhersin, V. C. Tran, J. Wallinga, T. Britton (2016). "Inferring R_0 in emerging epidemics - the effect of common population structure is small". *Journal of the Royal Society Interface*, **13**: 20160288.